GLOBAL BIOGEOCHEMICAL CYCLES, VOL. 15, No. 2, PAGES 483-506, JUNE 2001

Denitrification and N_2 fixation in the Pacific Ocean

Curtis Deutsch, Nicolas Gruber,[1] Robert M. Key, and Jorge L. Sarmiento

Program in Atmospheric and Oceanic Sciences, Princeton University, Princeton, New Jersey

Alexandre Ganachaud [2]

Massachusetts Institute of Technology/Woods Hole Oceanographic Institute Joint Program, Cambridge, Massachusetts

Abstract. We establish the fixed nitrogen budget of the Pacific Ocean based on nutrient fields from the recently completed World Ocean Circulation Experiment (WOCE). The budget includes denitrification in the water column and sediments, nitrogen fixation, atmospheric and riverine inputs, and nitrogen divergence due to the large-scale circulation. A water column denitrification rate of 48 $\pm$ 5 Tg N yr^{-1} is calculated for the Eastern Tropical Pacific using N^* [*Gruber and Sarmiento*, 1997] and water mass age tracers. On the basis of rates in the literature, we estimate sedimentary denitrification to remove an additional 15 $\pm$ 3 Tg N yr^{-1}. We then calculate the total nitrogen divergence due to the large scale circulation through the basin, composed of flows through a zonal transect at 32°S, and through the Indonesian and Bering straits. Adding atmospheric deposition and riverine fluxes results in a net divergence of nitrogen from the basin of -4 $\pm$ 12 Tg N yr^{-1}. Pacific nitrogen fixation can be extracted as a residual component of the total budget, assuming steady state. We find that nitrogen fixation would have to contribute 59 $\pm$ 14 Tg N yr^{-1} in order to balance the Pacific nitrogen budget. This result is consistent with the tentative global extrapolations of *Gruber and Sarmiento* [1997], based on nitrogen fixation rates estimated for the North Atlantic. Our estimated mean areal fixation rate is within the range of direct and geochemical rate estimates from a single location near Hawaii [*Karl et al.*, 1997]. Pacific nitrogen fixation occurs primarily in the western part of the subtropical gyres where elevated N^* signals are found. These regions are also supplied with significant amounts of iron via atmospheric dust deposition, lending qualitative support to the hypothesis that nitrogen fixation is regulated in part by iron suppy.

1. Introduction

Interest in the marine nitrogen cycle stems in large part from the fact that fixed nitrogen (all forms of nitrogen except N_2) is a limiting nutrient for biological growth over much of the world ocean [*Codispoti*, 1989; *Tyrell*, 1999]. The biologically mediated and globally dominant source and sink to the marine fixed nitrogen reservoir are nitrogen fixation and denitrification. Regions of the ocean in which denitrification and nitrogen fixation contribute most to the budget of fixed nitrogen are highly localized owing to various biological constraints on the organisms that carry out these processes.

Gaseous N_2 is fixed by organisms (called diazotrophs) that require large amounts of iron for the activation of nitrogenase, the enzyme responsible for breaking the strong triple bond of N_2. Diazotrophs are thus most commonly found in regions of high iron supply. In addition, the most prominent nitrogen fixer, *Trichodesmium sp.* is found to thrive only in waters warmer than 20°C and which are stably stratified [*Capone et al.*, 1997].

Denitrification is a metabolic process that is slightly less energetically favorable than aerobic respiration and is thus found to occur primarily in regions of low O_2 concentration. Significant marine denitrification occurs both in the sediments (usually on the continental margin) and in the subsurface waters of the open ocean

[1]Now at Institute of Geophysics and Planetary Physics, University of California, Los Angeles, CA

[2]Now at L'Institut Francais de Recherche pour l'Exploitation de la Mer, Plouzane, France

Paper number 2000GB001291.
0886-6236/01/2000GB001291$12.00

(usually in upwelling regions), where a combination of low O_2 supply and high productivity can create anoxic environments and a competitive advantage for denitrifying bacteria. Smaller components of the nitrogen budget include atmospheric and river inputs and losses to the sediments.

McElroy [1983] first proposed that because nitrogen is a limiting nutrient for biological growth, increases in the inventory of nitrogen during glacial periods could enhance the strength of the biological pump and reduce glacial atmospheric CO_2. This requires that changes in the relative magnitude of sources and sinks are capable of significantly changing the total N inventory on a glacial-interglacial timescale. In other words, it requires that the residence time of nitrogen in the ocean be of the order of a few thousand years. This is in line with recently revised nitrogen budget estimates by *Gruber and Sarmiento* [1997], which show a nitrogen cycle with large sources and sinks that are in approximate balance, giving a residence time for nitrogen of ~3000 years.

The original discussion by *McElroy* [1983] focused on the role of continental shelf sediment erosion in changing glacial-interglacial oceanic nitrogen inventory. Since then, however, two other mechanisms have been put forward. The first relies on changes in denitrification in two of the modern ocean's largest regions of water column denitrification. Studies have shown that the isotopic composition of nitrogen in the sediments of the Arabian Sea [*Altabet et al.*, 1995] and the Eastern Tropical Pacific [*Ganeshram et al.*, 1995] is lighter during glacial periods, indicating a weaker glacial denitrification sink in those two regions.

Alternatively, *Falkowski* [1997] and *Broecker and Henderson* [1998] have proposed that nitrogen fixation may play a large part in changing marine nitrogen and atmospheric CO_2 inventories. Indirect support for such a hypothesis comes from Antarctic ice core records, which show a decrease in dust flux prior to the increase in CO_2 at the last glacial termination [*Broecker and Henderson*, 1998]. Since much of the iron supply required by nitrogen fixers in the surface ocean is deposited in aeolian dust [*Duce et al.*, 1991], nitrogen fixation may have been reduced by a decrease in the dust supply. Acting alone, this would create an imbalance in sources and sinks that would reduce the nitrogen inventory and the ability of the biological pump to sequester CO_2. An increase in dust flux would have the opposite effect.

It is important to note that the proposed role of dust deposition and nitrogen fixation would not produce an immediate stimulation of global oceanic productivity during deglacial transitions. Rather, it would stimulate nitrogen fixation on a regional scale, which would increase global nitrogen availability on the timescale of deep ocean circulation. This is consistent with the relatively slow increase in ice core CO_2 that occurs after the change in dust supply [*Broecker and Henderson*, 1998].

These hypotheses are currently highly speculative. For example, the degree to which glacial-interglacial changes in denitrification and nitrogen fixation might be coupled is unknown. The ability to test whether such mechanisms may actually explain any significant portion of the glacial-interglacial atmospheric CO_2 change relies on understanding what controls the rates of nitrogen fixation and denitrification. Unfortunately, the magnitudes and controls of these processes, especially pelagic nitrogen fixation, are rather poorly known in the modern ocean. The global N_2 fixation rate in the budget of *Gruber and Sarmiento* [1997], for example, was crucial to their estimate of the residence time of oceanic N but was tentatively extrapolated from areal rates estimated in the North Atlantic.

In this study, we extend to the Pacific Ocean the approach developed by *Gruber and Sarmiento* [1997] for mapping regions of marine nitrogen fixation and denitrification and for calculating basin-scale rates of these processes. This approach is based on a quasi-conservative tracer N*, which is a linear combination of nitrate (N) and phosphate (P), as will be described in section 2 of this paper. Section 3 consists of a description and discussion of the Pacific N* distribution and what it tells us qualitatively about the Pacific nitrogen cycle. In section 4 we provide a nitrogen budget based on N* and age tracer fields, together with transport estimates at boundaries of the basin. We conclude in section 5 with a summary and outlook.

2. Methods and Concept of N*

The derivation and concept of N* have been discussed in detail by *Gruber and Sarmiento* [1997]. A slightly modified and generalized presentation will be given here.

We assume that the biological pump, which makes the largest contribution to the spatial variability of oceanic N, may be decomposed into two components. The first we call the normal biological pump, in which N and P are consumed and released with the same constant ratio, $r_{\mathrm{nitr}}^{\mathrm{N:P}}$. The second consists of nitrogen fixation and denitrification, in which N and P are assimilated and remineralized with N:P ratios different than $r_{\mathrm{nitr}}^{\mathrm{N:P}}$. These stoichiometric differences suggest the definition of the tracer $\mathrm{N}^* = \mathrm{N} - r_{\mathrm{nitr}}^{\mathrm{N:P}}\,\mathrm{P}$, which would be unchanged by the normal biological pump, allowing us to trace that part of the oceanic N variability that is due to denitrification and nitrogen fixation.

We derive here a general continuity equation for N*, from the continuity equations for N and P, which are

$$\Gamma(\mathrm{N}) = J_{\mathrm{nitr}}(\mathrm{N}) + J_{\mathrm{denit}}(\mathrm{N}) + J_{\mathrm{N\text{-}rich}}(\mathrm{N}), \qquad (1)$$

$$\Gamma(\mathrm{P}) = J_{\mathrm{nitr}}(\mathrm{P}) + J_{\mathrm{denit}}(\mathrm{P}) + J_{\text{N-rich}}(\mathrm{P}) + J_{\mathrm{up\ nf}}(\mathrm{P}). \quad (2)$$

The operator Γ represents the transport and time rate of change, $\Gamma() = \partial()/\partial t + \vec{u}\cdot\nabla() - \nabla\cdot(D\cdot\nabla())$, where $\vec{u}$ is the velocity field, and D is the eddy diffusivity. The J terms denote the sources minus sinks due to (in order of appearance) the normal biological pump, denitrification, remineralization of N-rich organic matter from diazotrophs, and uptake (of P only) by nitrogen fixers. These equations are similar to those used by *Gruber and Sarmiento* [1997]. We have added the $J_{\mathrm{up\ nf}}(\mathrm{P})$ term in order to consider processes over the entire water column. *Gruber and Sarmiento* [1997] focused on the remineralization of N and P and therefore did not include this P uptake term.

We assume that the N sink and P source due to denitrification have a constant N:P ratio, $r^{\mathrm{N:P}}_{\mathrm{denit}} = -104$, given by the reaction equation for denitrification coupled with the mineralization of organic matter with the stoichiometry of *Anderson* [1995]:

$$\mathrm{C_{106}H_{175}O_{42}N_{16}P} + 104\,\mathrm{NO_3^-} = 4\,\mathrm{CO_2} + 102\,\mathrm{HCO_3^-} + 60\,\mathrm{N_2} + 36\,\mathrm{H_2O} + \mathrm{HPO_4^{2-}} \quad (3)$$

We can relate the N and P source terms of denitrification by $J_{\mathrm{denit}}(\mathrm{N}) = r^{\mathrm{N:P}}_{\mathrm{denit}}\, J_{\mathrm{denit}}(\mathrm{P})$ and of the normal biological pump by $J_{\mathrm{nitr}}(\mathrm{N}) = r^{\mathrm{N:P}}_{\mathrm{nitr}} J_{\mathrm{nitr}}(\mathrm{P})$. Then the N and P continuity equations can be combined as $\Gamma(\mathrm{N}) - r^{\mathrm{N:P}}_{\mathrm{nitr}}\Gamma(\mathrm{P})$ to yield

$$\Gamma(\mathrm{N^*}) = J_{\mathrm{denit}}(\mathrm{N}) - \left(\frac{r^{\mathrm{N:P}}_{\mathrm{nitr}}}{r^{\mathrm{N:P}}_{\mathrm{denit}}}\right) J_{\mathrm{denit}}(\mathrm{N}) + J_{\text{N-rich}}(\mathrm{N}) - r^{\mathrm{N:P}}_{\mathrm{nitr}}\left[J_{\text{N-rich}}(\mathrm{P}) + J_{\mathrm{up\ nf}}(\mathrm{P})\right]. \quad (4)$$

Substituting stoichiometric N:P values of $r^{\mathrm{N:P}}_{\mathrm{nitr}} = 16$ and $r^{\mathrm{N:P}}_{\mathrm{denit}} = -104$ and adding a constant 2.90 μmol kg^{-1} to the definition of N* to give a global mean of 0 gives

$$\mathrm{N^*} = \mathrm{N} - 16\mathrm{P} + 2.90\ \mu\mathrm{mol\ kg^{-1}}, \quad (5)$$

$$\Gamma(\mathrm{N^*}) = 1.15\, J_{\mathrm{denit}}(\mathrm{N}) + J_{\text{N-rich}}(\mathrm{N}) - 16\,\left[J_{\text{N-rich}}(\mathrm{P}) + J_{\mathrm{up\ nf}}(\mathrm{P})\right]. \quad (6)$$

Some comments concerning these equations are in order. First, N* is unchanged by the normal biological pump, leaving denitrification and nitrogen fixation as the sole sink and source of N* (contributions from the atmosphere and rivers are accounted for in the transport term, $\Gamma(N^*)$).

Second, since denitrification changes N and P with a ratio less than $r^{\mathrm{N:P}}_{\mathrm{nitr}}$, it is an N* sink and will be revealed by low N* anomalies. Denitrification is represented by the first two terms on the right hand side of (4): the first term is the sink of N* from the direct loss of N, whereas the second term represents the loss of fixed nitrogen from the organic nitrogen pool. This can be seen from the stoichiometry of (3), in which the denitrification P source is related to the loss of TON by the N:P ratio of organic matter. The denitrification stoichiometry can be expressed as

$$\left(\frac{r^{\mathrm{N:P}}_{\mathrm{nitr}}}{r^{\mathrm{N:P}}_{\mathrm{denit}}}\right) J_{\mathrm{denit}}(\mathrm{N}) = r^{\mathrm{N:P}}_{\mathrm{nitr}} J_{\mathrm{denit}}(\mathrm{P}) = -J_{\mathrm{denit}}(\mathrm{TON}). \quad (7)$$

This shows that the second term in (4) is identical to a conversion of TON to N_2 during denitrification. The two terms have been combined in (6).

Finally, both the uptake of P by diazotrophs (without N uptake) and the remineralization of their N-rich organic matter are sources of N* and will be revealed by high N* anomalies. These processes are represented by the remaining terms in (4), and their relative magnitudes will determine the net N* signal resulting from nitrogen fixation. This will be discussed further in section 4.

It should be noted that the constant in (5) involves no assumptions about the balance between nitrogen fixation and denitrification; it simply allows us to easily identify high and low anomalies relative to the global mean. In this sense, the absolute value of N* is arbitrary. Negative (positive) values of N* cannot be directly associated with denitrification (nitrogen fixation). Only deviations from conservative behavior are meaningful in identifying regions of denitrification and nitrogen fixation.

Two small differences exist between our derivations and those of *Gruber and Sarmiento* [1997], who defined an N* equivalent to ours, but divided both N* and its continuity equation by 1.15 to eliminate the coefficient from the $J_{\mathrm{denit}}(\mathrm{N})$ term. We prefer to retain this coefficient in the continuity equation rather than in the definition of N*, in part because a multiplicative constant in the definition of N* leads to confusion. Furthermore, the additional factor of 0.15 multiplying the denitrification sink term has geochemical significance as noted above, representing the portion of nitrogen loss from the organic reservoir. These changes have no effect on the results and conclusions of *Gruber and Sarmiento* [1997].

Finally, because our N* continuity equation (6) includes the effect of P uptake by nitrogen fixers, it is slightly more general than that of *Gruber and Sarmiento* [1997]. It is valid over the entire water column, rather than just below the euphotic zone. The general continuity equation (6) will be explored more fully in section 4, for two specific cases relevant to establishing the nitrogen budget.

3. Pacific N* Distribution

The use of N* to investigate the nitrogen cycle requires a nutrient data set of high quality, since N* is a small difference between highly correlated concentra-

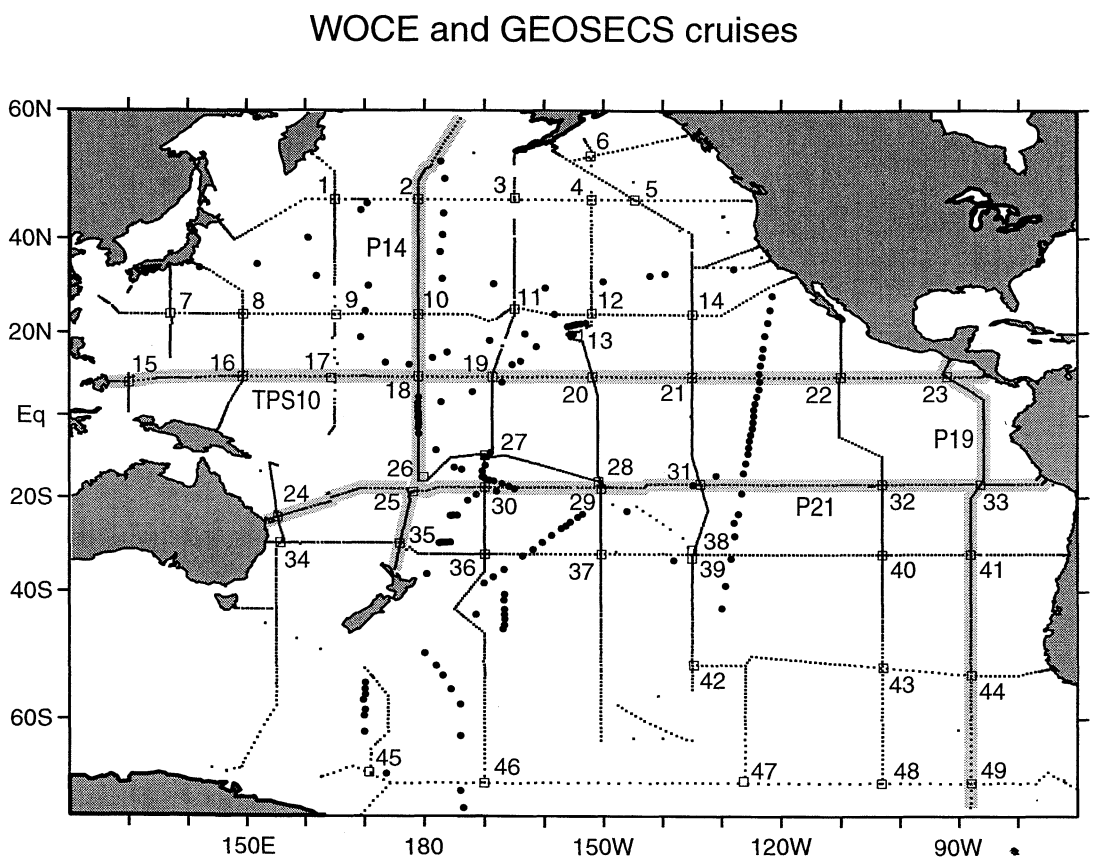

Figure 1. Map of station locations for data used in this study. WOCE cruises are indicated by the grid-like array of small dots; Geochemical Ocean Sections (GEOSECS) stations (used for mapping purposes only) are indicated by larger circles. For cruise information see Table 5.

tions. Such a data set for the Pacific has recently become available through the WOCE program. The spatial distribution of WOCE stations used for this study is shown in Figure 1, along with stations from the Geochemical Ocean Sections Study (GEOSECS). Before combining data from individual cruises, the internal consistency of the data was examined and "corrections" were applied to two cruises, as explained in appendix A. Assuming that errors in measurement of N and P are independent and of magnitude 0.1 and 0.01 μmol kg^{-1}, respectively, the resulting analytical error in N* is $\sim$0.2 μmol kg^{-1}.

Mean vertical profiles from four regions of the Pacific, the Eastern Tropical North and South Pacific (ETNP, ETSP), and the western part of the northern and southern subtropical gyres, are shown in Figure 2. All four profiles show high N* values at the surface that decrease rapidly with depth to local minima in the top 1000 m. Surface maxima are higher in the west, and subsurface minima are lower and sharper in the east. The vertical gradients and range of values are much greater in the north than in the south. These profiles capture many of the primary features of the Pacific N* distribution, which are large high anomalies in the near-surface waters of the western subtropical gyres and low anomalies in the oxygen minimum zones of the Eastern Tropical thermocline.

We investigate the distribution of N* more fully with two zonal and two meridional sections, shown in Figures 3-6. The zonal section from the TPS10 cruise at 10°N (Figure 3) shows that the vertical N* minimum in the thermocline is a feature that persists across the entire basin. The depth of the vertical minimum increases westward from less than 500 m at the North American coast to $\sim$1000 m at 130°E, while N* values simultaneously increase (the minimum weakens) from concentrations below -15 to about -3 μmol kg^{-1} (note that the lowest values do not show up in the objective mapping due to smoothing). Similar features can also be seen in the southern section along 17°S from the P21 cruise (Figure 4). In addition, the southern section shows a second distinct vertical minimum in the east. This deep N* minimum is coincident with a minimum in ^{14}C characteristic of the relatively old North Pacific Deep Water [*Key et al.*, 1996]. The broad southward return flow of North Pacific Deep Water observed here

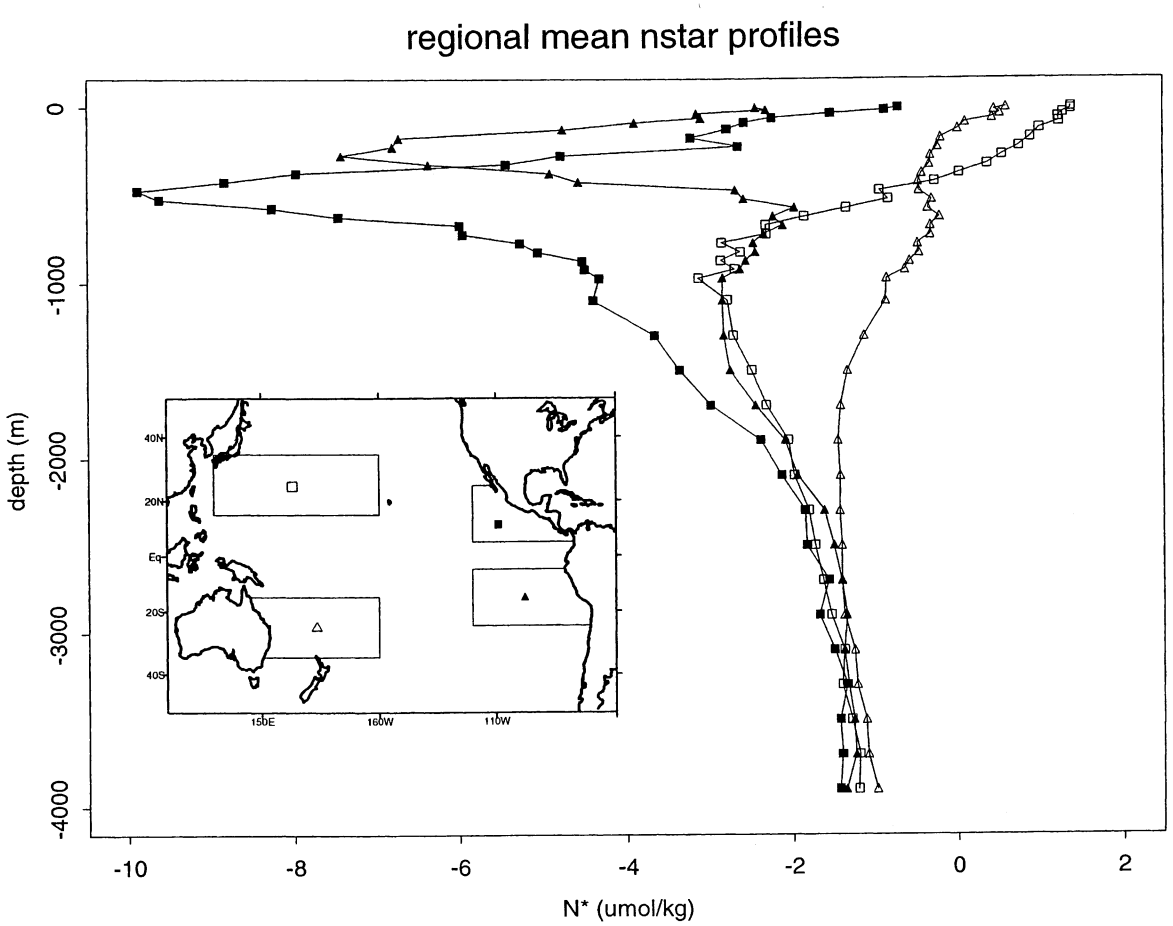

Figure 2. Average vertical N* profiles for four regions, the Eastern Tropical North and South Pacific and the northern and southern subtropical gyres. The regions and their plotting symbols are indicated on the inset map.

likely obtains its N* signature from the low N* waters of the Subarctic Pacific (see also Figures 5-6). In both sections, high N* concentrations at the surface in the west decrease to deep water values within the top few hundred meters. Deep waters (below 2000 m) throughout the Pacific have roughly constant N* of -1 to -2 μmol kg^{-1}.

Two meridional sections, through the Eastern Pacific (cruise P19, 90°W) and Western Pacific (cruise P14, 180°) are shown in Figures 5-6, respectively. The eastern section is dominated by the distinct low anomalies of the ETNP and ETSP and by a subsurface maximum south of 30°S. The high N* values correspond to Antarctic Intermediate Water, which flows beneath the core of the ETSP N* minimum (see also Figure 2). Under the Antarctic Intermediate Water lies the second vertical N* minimum of North Pacific Deep Water seen in Figure 4. The continuity between this deeper N* minimum and northern N* minima (see also Figure 6) further suggests that the signal is a result of mixing with northern denitrified waters. An expansive low N* anomaly can be seen in the western section (Figure 6) extending from surface to bottom north of 46°N and into the Bering Sea. This feature also extends south of 30°N at middepths of 1000-2000 m, creating sharp vertical and horizontal gradients in the upper water column between 30°N-40°N. In the western section, the two bowl-shaped high N* regions centered at 25°N and 30°S reveal the latitudinal extent of the surface maxima seen in profiles there.

Maps of N* along horizontal and isopycnal surfaces (Figures 7-8) show several interesting large-scale features. The highest N* values anywhere in the Pacific are found in the near-surface waters in the western part of the northern subtropical gyre, with secondary highs found in the southern subtropical gyre off the Australian continent (Figure 7). The broad scale of these N* maxima indicate that nitrogen fixation is an important process in these regions. Comparison of Figures 8a and 8b show that maximum N* values and their horizontal extent are reduced on deeper surfaces, a result of the decrease with depth of N-rich organic matter being remineralized.

The chemical front coincident with the Kuroshio cur-

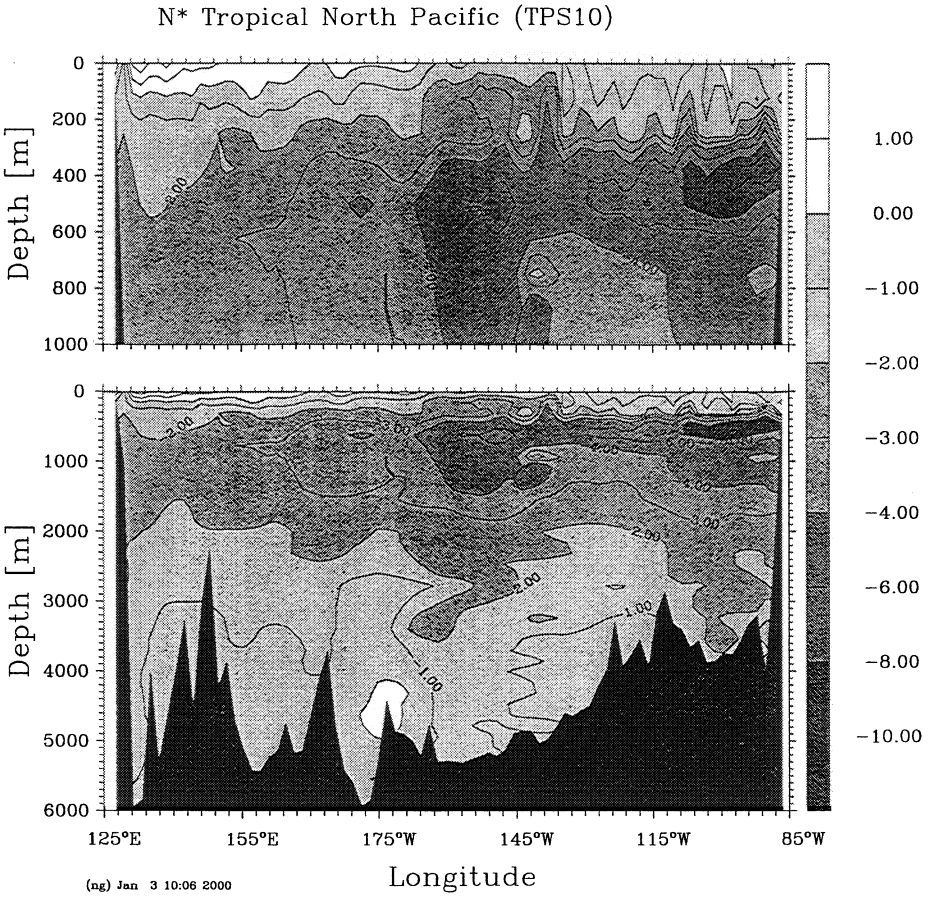

Figure 3. Zonal section of N* (μmol kg^{-1}) along 17°S based on data from the WOCE P21 cruise. See Figure 1 for station locations. All sections were prepared using the objective mapping procedure described by *Gruber and Sarmiento* [1997] .

rent (Figure 6) divides the high N* waters of the subtropical gyre from the the low N* waters of the Subarctic Pacific. Denitrification is known to occur in the expansive shelf sediments of the Bering Sea [*Koike and Hattori*, 1979; *Tsunogai et al.*, 1979; *Haines et al.*, 1981], and may give rise to the low N* values observed there. Note that N* cannot distinguish between denitrification in the water column and sediments.

Horizontal N* minima (Figure 8) are found in the Eastern Tropical Pacific, where two distinct low N* regions with values well below -10 μmol kg^{-1} extend westward from the American coasts along axes at 15°N in the ETNP and 15°S in the ETSP. Equatorial waters separate the two regions with a ridge of N* values above -1 μmol kg^{-1}. The oxygen values in the core of the N* minima reach nearly undetectable levels, making the ETNP and ETSP ideal environments for denitrification, as was first recognized by *Brandhorst* [1959] (see *Hattori* [1983] for a review).

The N* minima propagate well into the western Pacific. Values below -4 μmol kg^{-1} can be found as far west as 160°W in the north and 150°W in the south, even though oxygen levels there would strongly inhibit denitrification. The shape and position of these tongues, together with the high O_2 values, suggest that the zonal extent of the low N* anomalies is an advective feature, owing to the entrainment of denitrified water by the North and South Equatorial Currents. These westward currents carry the low N* signal into the subtropical gyres before being mixed away by high N* waters traveling east from the western side of the basin in the equatorial countercurrents. This explains why profiles from regions with such different nitrogen dynamics as the subtropical gyre and the Eastern Tropical Pacific, can have such similar vertical structure (see Figure 2). The coupling of the N* signal between regions of denitrification and regions of nitrogen fixation is testament to the care that must be taken in interpreting

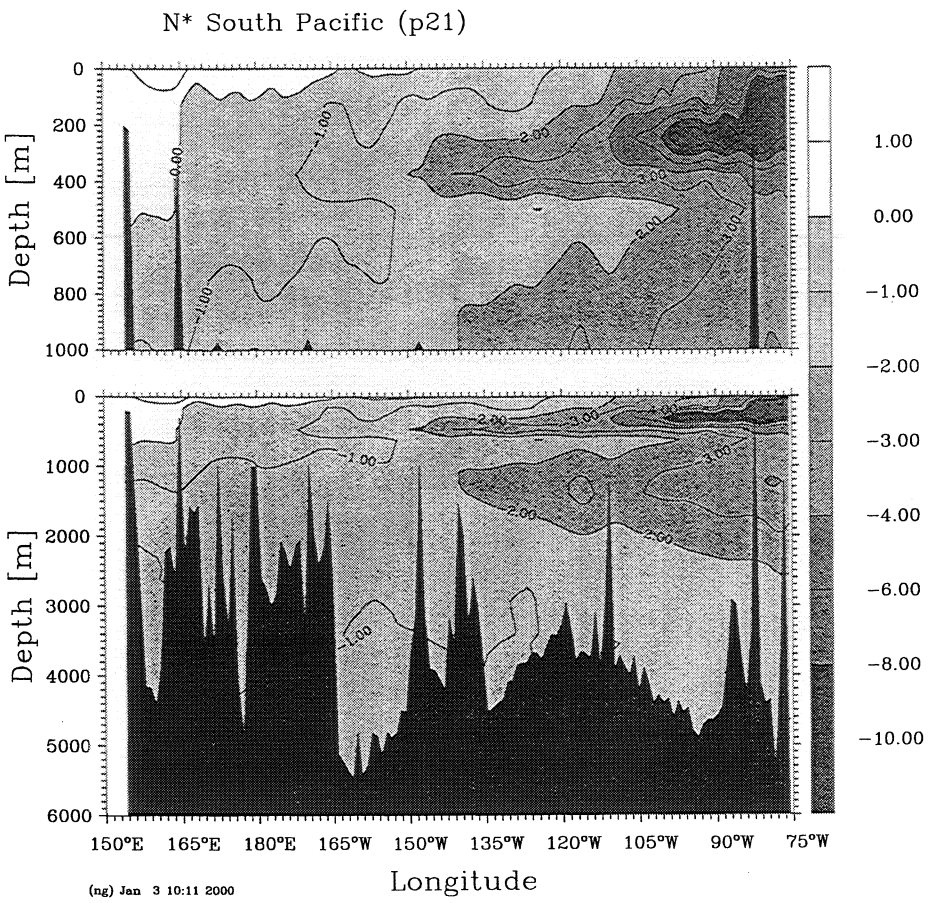

Figure 4. Zonal section of N* (μmol kg^{-1}) along 10°N based on data from the TPS10 cruise. See Figure 1 for station locations.

local N* signals, which are due to nitrogen fixation and denitrification as well as transport and mixing processes experienced by a water parcel over its history.

4. Budget

We now return to the general N* continuity equation (6) and examine two specific cases in which we can use it to obtain information about sources and sinks of fixed nitrogen. The first case is for waters below the depth of P uptake by diazotrophs. We then have $J_{\text{up nf}}(\text{P}) = 0$, and the $J_{\text{N-rich}}(N, P)$ terms can be combined assuming a constant stoichiometry: $J_{\text{N-rich}}(\text{N}) = r^{\text{N:P}}_{\text{N-rich}}\, J_{\text{N-rich}}(\text{P})$. The value of $r^{\text{N:P}}_{\text{N-rich}}$ is highly variable, ranging from ratios near 16 (Doug Capone, personal communication, 2000) to 125 [*Karl et al.*, 1992]. Although the estimates of this study will be independent of $r^{\text{N:P}}_{\text{N-rich}}$, the value 125 used by *Gruber and Sarmiento* [1997] yields

$$\begin{aligned}\Gamma(\text{N}^*) &= \left(1 - \frac{r^{\text{N:P}}_{\text{nitr}}}{r^{\text{N:P}}_{\text{denit}}}\right) J_{\text{denit}}(\text{N}) \\ &\quad + \left(1 - \frac{r^{\text{N:P}}_{\text{nitr}}}{r^{\text{N:P}}_{\text{N-rich}}}\right) J_{\text{N-rich}}(\text{N}) \\ &= 1.15\, J_{\text{denit}}(\text{N}) + 0.87\, J_{\text{N-rich}}(\text{N}). \qquad (8)\end{aligned}$$

This is identical to equation (14) of *Gruber and Sarmiento* [1997], aside from the rearrangement of multiplicative constants as noted in section 2. This equation, valid when remineralization is the only biological transformation occuring, relates changes in N* concentration to the net effects of denitrification, the remineralization of organic matter from diazotrophs, and mixing.

A second case of interest arises when the uptake and remineralization of P from diazotrophs are in balance. To a first approximation, this will be satisfied when (6) is integrated over the entire water column. To be

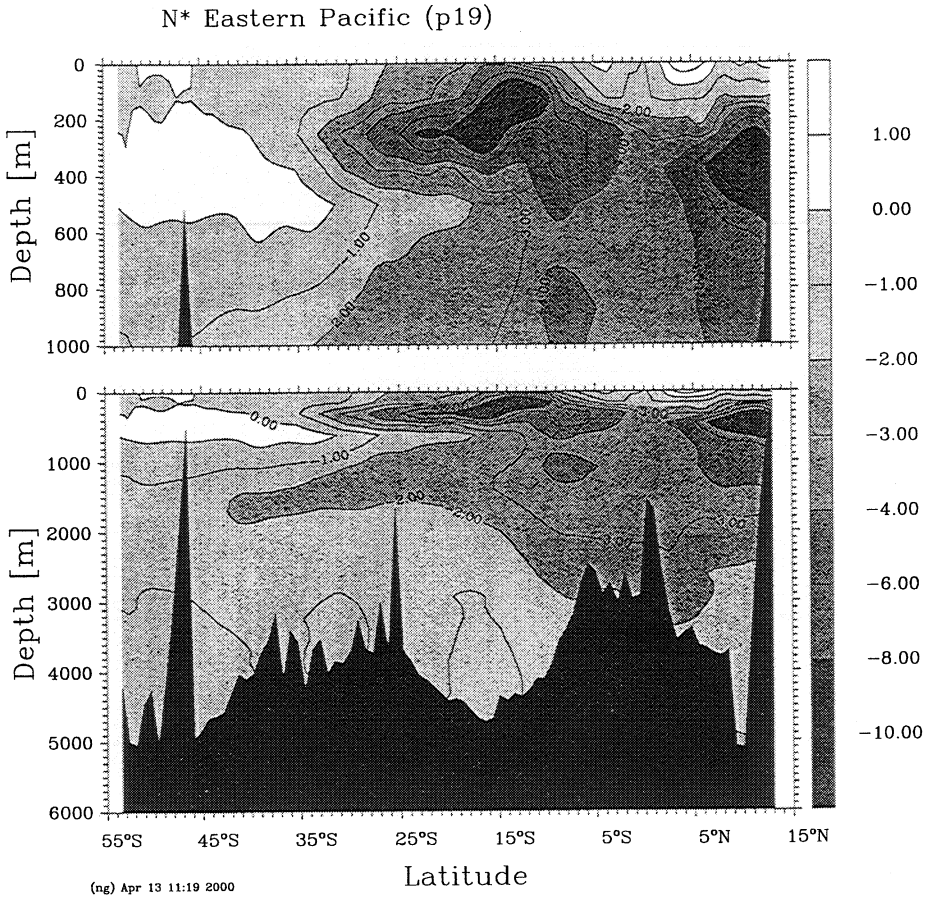

Figure 5. Meridional section of N* (μmol kg^{-1}) along 90°W based on data from the WOCE P19 cruise. See Figure 1 for station locations.

strictly valid, all diazotrophic organic matter formed in the region must also be remineralized there.

Integrating (6) in steady state over a region where the formation and remineralization of N-rich organic matter are balanced (i.e., $\int_V [J_{\text{up nf}}(\text{P}) + J_{\text{N-rich}}(\text{P})]\, dV = 0$), we obtain

$$\int_S \Gamma(\text{N}^*)\, dS = \int_S [\Gamma(\text{N}) - 16\,\Gamma(\text{P})]\, dS = \int_V [1.15 J_{\text{denit}}(\text{N}) + J_{\text{N-rich}}(\text{N})]\, dV, \quad (9)$$

which states that the volume-integrated sources and sinks of N due to nitrogen fixation and denitrification within the region are balanced by a flux divergence of N* across its boundaries. Notice that the first equality holds if there is no net mass divergence, so that the arbitrary constant in the definition of N* makes no contribution to N* divergence. Notice also that this equation is independent of the poorly known value of $r^{\text{N:P}}_{\text{N-rich}}$. Further explanation and interpretation of (9) is provided in appendix B.

Equations (8) and (9) relate sources and sinks of N to the transport of N*. They will be used in the following subsections to construct a nitrogen budget for the Pacific Ocean. We begin in subsection 4.1, by using (8) along with water mass age tracers and N* to calculate spatially and temporally integrated rates of denitrification in the N* minima of the Eastern Tropical Pacific. We then constrain the magnitude of nitrogen fixation, by using (9) with an estimate for N* divergence in the Pacific. We conclude with a summary of the resulting budget.

4.1. Denitrification in the Eastern Tropical Pacific

A water parcel in which denitrification (nitrogen fixation) is occuring will show N* anomalies that decrease or (increase) with time. If we remove the effects of mixing between water masses, we can use N* with water mass ages to estimate rates of the two processes. Here we use CFC-12 as the age tracer (see appendix C) to estimate denitrification in the eastern tropical Pacific.

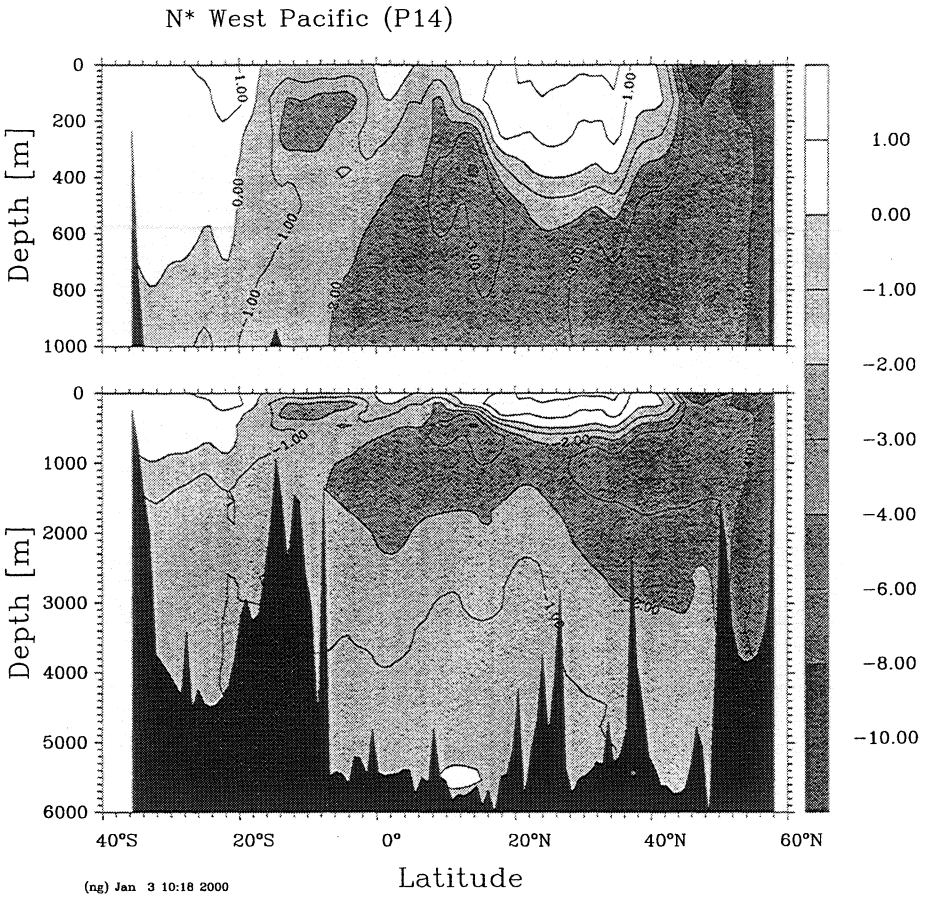

Figure 6. Meridional section of N* (μmol kg^{-1}) along 180°, based on data from the WOCE P14 cruise. See Figure 1 for station locations.

If the relative contributions of each source water type in a mixture are known, then the value of N*, age, and salinity for every sample can be decomposed into contributions from mixing of source waters and a residual value due to nonconservative processes [*Anderson and Sarmiento*, 1994]. For the general case of n, source water types whose relative volumetric contributions to the mixture, and characterisic N*, age, and salinity values are indicated by f_i, N_i^*, τ_i, and S_i, respectively.

$$1 = \sum_{i=1}^{n} f_i, \tag{10}$$

$$S = \sum_{i=1}^{n} f_i \, S_i, \tag{11}$$

$$N^* = \sum_{i=1}^{n} f_i \, N_i^* + \Delta N^*, \tag{12}$$

$$\tau = \sum_{i=1}^{n} f_i \, \tau_i + \Delta\tau. \tag{13}$$

Here the nonconservative component in the mixing of N* (ΔN^*), represents the cumulative effect of a source or sink of N* during the time interval since the end members left their locations of origin. In turn, that time interval is given by the increase in the age, $\Delta\tau$. Having thus removed the effect of mixing on N* and age, the mean rate of net N losses/gains due to nitrogen fixation and denitrification in the parcel is

$$\frac{\Delta N^*}{\Delta\tau} = \overline{1.15\, J_{\text{denit}}(\text{N}) + 0.87\, J_{\text{N-rich}}(\text{N})}\Big|_{\Delta\tau}. \tag{14}$$

We use a two end-member mixing model because it represents well the circulation regime in the eastern tropical Pacific [*Wyrtki*, 1967]. The subsurface circulation in the tropical Pacific is highly variable on both seasonal and interannual timescales. However, on average, the eastern waters find their origin primarily in the high salinity, low oxygen waters of the equatorial counter current that diverges around the Galapagos islands, spreading north and south. A second distinct

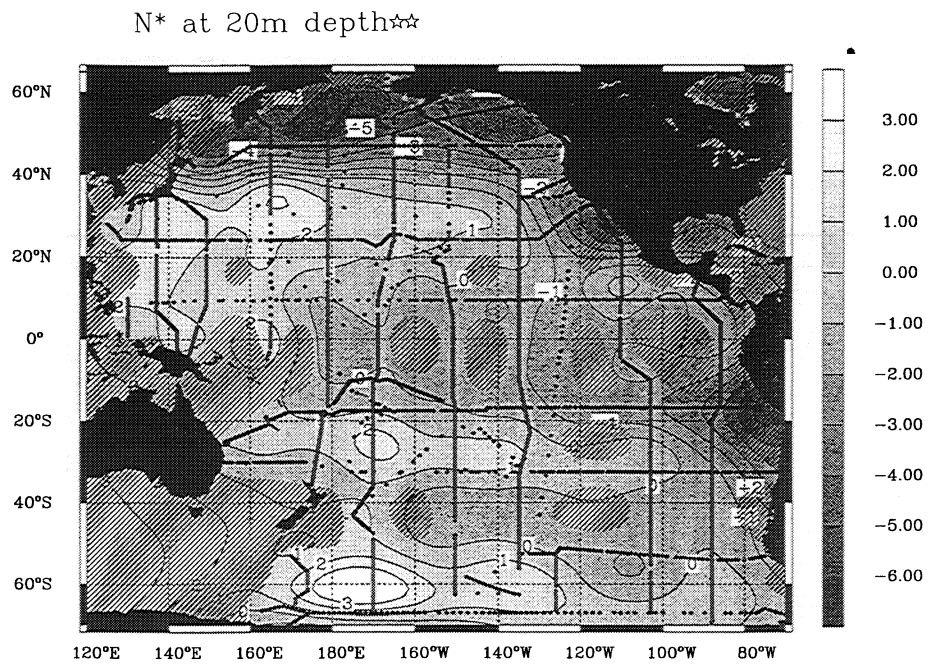

Figure 7. Map of N* (μmol kg^{-1}) linearly interpolated to the 20 m depth surface. All maps were prepared using the objective mapping technique described by *LeTraon* [1990]. Dashed areas indicate where the interpolation error in N* from the objective mapping procedure is > 20%.

water type comes from the broad, low salinity, equatorward flow on the eastern side of the subtropical gyres. These flows separate from the American coasts near the poleward boundaries of the low N* tongues, turning west into the north and south equatorial currents.

We assume that these two water masses mix predominantly along isopycnal surfaces, and select for analysis, data on 8 isopycnal layers containing the N* minimum. For each isopycnal layer, we first choose end-member characteristics based on plots of age and N* versus salinity. Source water fractions f_1 and f_2 are calculated from the salinity mixing equation subject to the mass conservation constraint (equations (10) and (11)). Finally, ΔN^* and $\Delta\tau$ are calculated according to (12) and (13). Assuming that the contribution of nitrogen fixation in these regions is negligible, the slope of the best fit line for ΔN^* versus $\Delta\tau$ (equation (14)) gives the mean denitrification rate in the region, over the time since the water masses left their end-member locations.

Figure 9 provides an example for one layer in the ETSP. Plots of salinity versus N* and age show the characteristic "bowing" of two end-members mixing with a nonconservative parameter. The end members chosen for each isopycnal are listed in Table 1. In contrast, plots of N* and CFC-age for the ETNP (Figure 10) reveal a very homogenous water mass, with almost no variation in salinity. This indicates a negligible influence of the low salinity waters from the northern gyre. That is, the ETNP is well described by a single end-member.

However, some stations in the ETNP, located just off the southern tip of Baja California, show a significant low salinity input as well as much lower N* values, placing them well off the main trend in N* versus CFC-age. Owing to the clear low salinity input, the relatively northern location and the distinct N* values of these points, we interpret these waters as having experienced a longer history of denitrification relative to the main data cluster. This is supported by the data upstream from the low N* region, along the California coast. Depth profiles of N* for stations in the upstream region along 35°N show stronger near-bottom gradients as stations approach the continental shelf due to the denitrification that has been observed in sediments there [*Barnes et al.*, 1975; *Jahnke et al.*, 1990].

We thus interpret the water at stations off Baja California as being of northern origin and as having acquired a shelf denitrification signal by mixing with shelf waters. Since we are only considering water column denitrification here, we discard these points for the rate calculation and consider only those points that have not mixed with previously denitrified waters from the north. Since the remainder of ETNP water is well described by a single water type, we calculate the rate of denitrification in this region as simply the slope of the N* versus age plot.

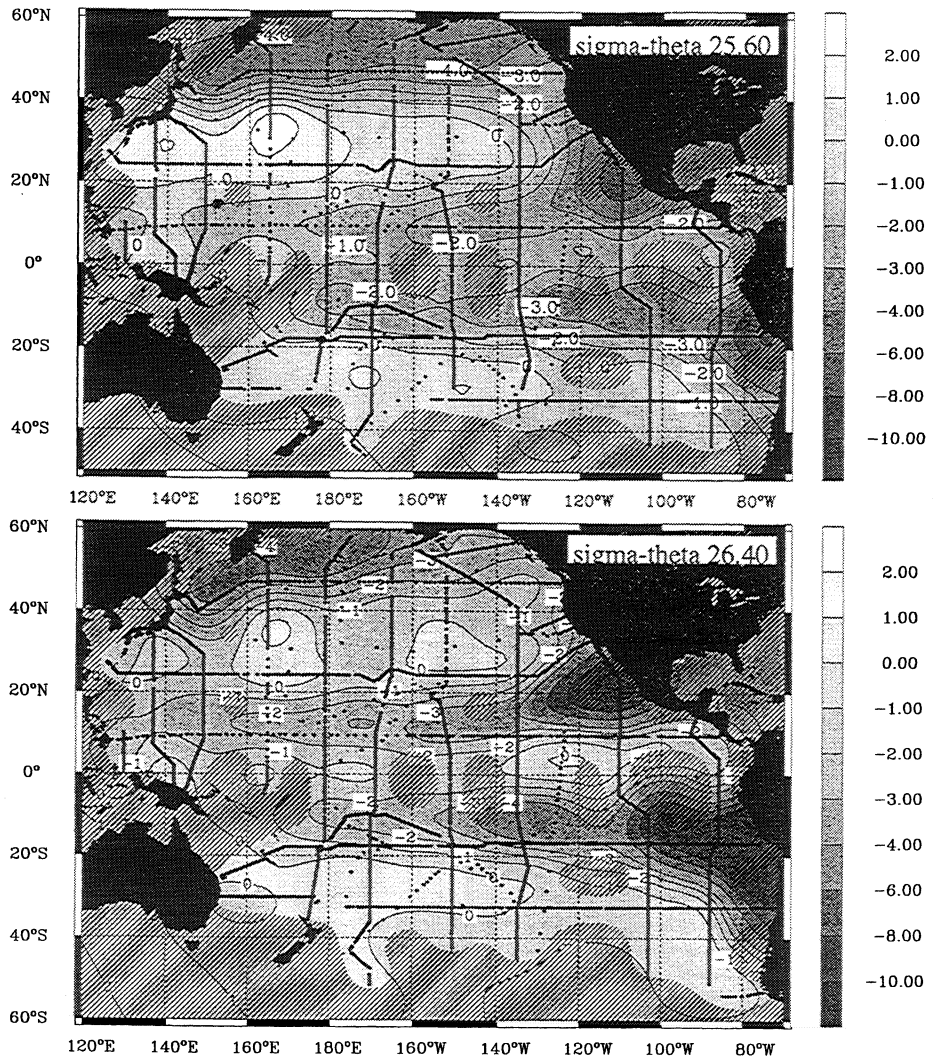

Figure 8. Map of N* (μmol kg^{-1}) in the thermocline on two isopycnal surfaces, prepared as in Figure 7. (a) Sigma-theta 25.6 is located at depths of 200-300 m in the subtropical gyres, shoaling to ~100 m in the east; (b) sigma-theta 26.4 is found at depths of 400-500 m in the gyres decreasing to ~200 m toward the east and in the equatorial band.

The mass specific rates are given in Table 2. Denitrification in the ETSP reaches a maximum rate of 2.5 μmol kg^{-1} yr^{-1} on the sigma-theta 26.2 surface (~250 m), which is colocated with the vertical minimum of N*. The ETNP denitrification rates increase toward the bottom of the investigated depth range. This depth range was constrained by the CFC-aging technique to the top ~500 m, since below that depth CFC-ages exceed 40 years (see appendix C). Notice that mass specific rates are an order of magnitude smaller in the north than in the south.

These rates are then integrated over the volume of each isopycnal layer within the denitrification zones, as calculated using the NOAA NESDIS atlas [*Levitus et al.*, 1994; *Levitus and Boyer*, 1994]. The boundaries of the denitrification zones are taken to approximate the 20 μmol kg^{-1} isoline of oxygen (roughly from the coast to 110°W and from 10°S-25°S in the south and from 10°S-20°N in the north). Integrated denitrification rates for both regions are plotted versus density in Figure 11. We calculate a net nitrogen loss of 26 ± 4 Tg N yr^{-1} for the ETSP and 11 ± 1.7 Tg N yr^{-1} for the ETNP.

The inherent limitations of the CFC-age tracer do not allow us to directly estimate the total nitrogen loss in the ETNP. However, a study of in situ denitrification by *Codispoti and Richards* [1976], found half of the denitrifying layer to be below sigma-theta 26.8. We therefore double our estimate of nitrogen loss in the ETNP from 11 to 22 ± 3.5 Tg N yr^{-1} to account for the lower half

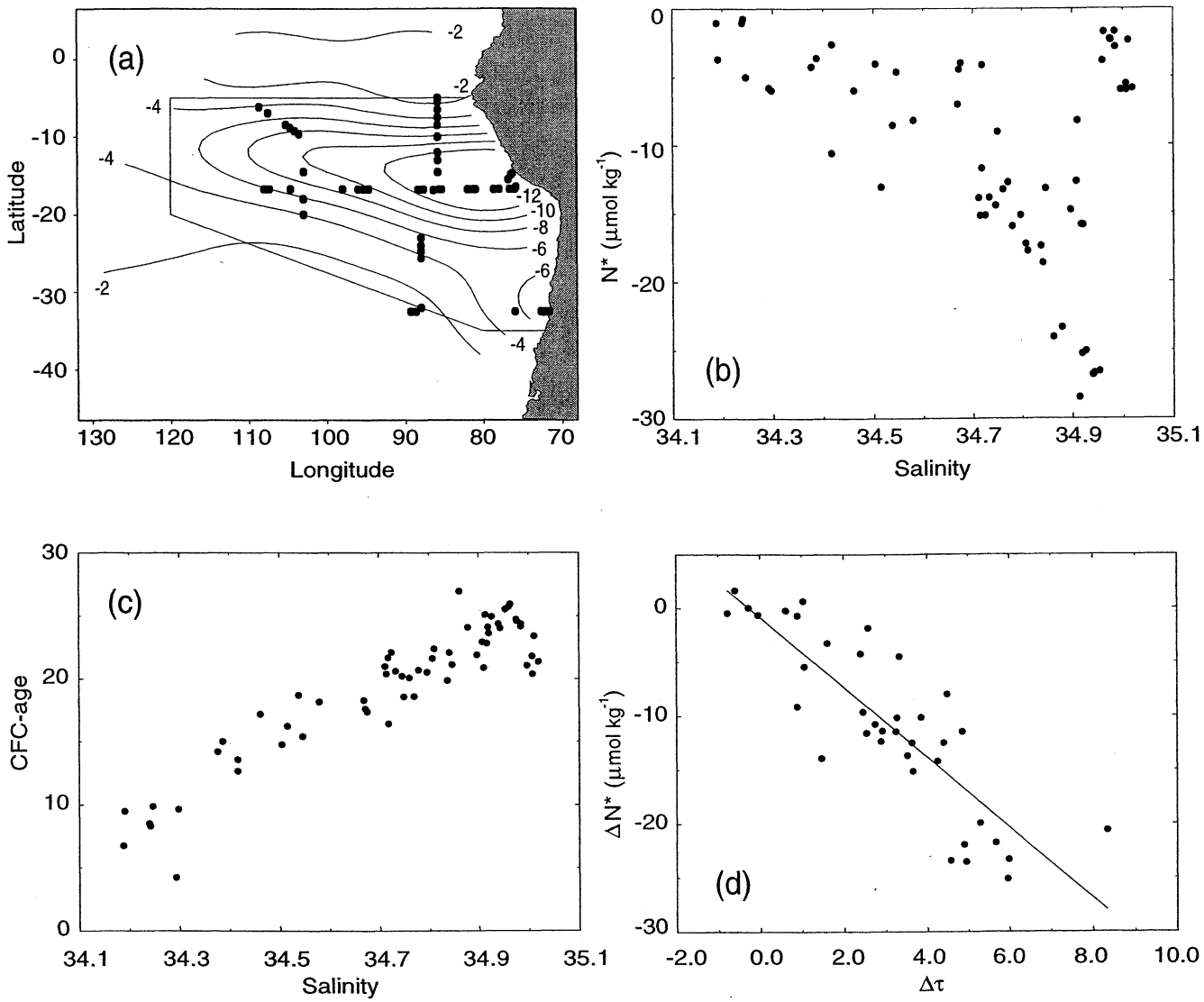

Figure 9. Data used for denitrification rate calculation on sigma-theta 26.2 in the ETSP. (a) Contours of N* with locations of stations having both N* and CFC-12 values in the specified density interval are shown. (b) N* and (c) CFC-age versus salinity are shown, respectively. (d) The slope gives the mass specific denitrification rate (see equation (8)).

of the denitrification zone. Although the mass specific rates of denitrification in the north are much smaller than in the south, the volume of the denitrification region in the north is sufficiently larger to make the total N loss comparable in both regions.

Our estimate of the total N loss for water column denitrification in the Pacific is 48 ± 5 Tg N yr^{-1}. This result is quite close to previous studies that used very different techniques (see Table 3). *Codispoti and Packard* [1980], *Tsunogai* [1971], and *Codispoti and Richards* [1976] extrapolated in situ measurements of the electron transfer activity associated with nitrate reduction, to arrive at rates of denitrification in both the northeast and southeast tropical Pacific of 18-26 Tg N yr^{-1}. *Codispoti and Richards* [1976] also estimated the integrated nitrate loss in the ETNP based on the diffusion and geostrophic transport of nitrate deficits out of the ETNP. Our estimates of denitrification are in the range of all of these previous estimates despite the wide variety of methods.

4.2. Nitrogen Fixation

We attempted to apply the above method to the high N* regions of both the northern and southern subtropical gyres, without success. Neither 1, 2, or 3 endmember mixing models revealed an increase in excess nitrogen with age. This is in contrast to the North Atlantic, where *Gruber and Sarmiento* [1997] were able

Table 1. End-Member Characteristics on Isopycnal Surfaces in the ETSP

Isopycnal Layer		End-Member Composition					
Midval	Interval μmol kg^{-1}	N_1^*, μmol kg^{-1}	N_2^*,	S_1	S_2 year	τ_1, year	τ_2,
25.80	25.65–25.95	-1.0	-3.0	34.40	35.35	5	6
26.05	25.95–26.15	-1.0	-4.0	34.30	34.95	9	12
26.20	26.15–26.25	-4.0	-5.0	34.40	35.00	14	21
26.30	26.25–26.35	-2.0	-5.0	34.20	35.00	13	25
26.40	26.35–26.45	-6.0	-4.0	34.37	34.93	17	25
26.50	26.45–26.55	-7.0	-2.0	34.55	34.89	24	30
26.60	26.55–26.65	-8.0	-2.0	34.55	34.84	25	33

to identify the signal without difficulty. Several factors may be responsible for this difference.

As described in section 3, N* maxima in the subtropical western Pacific are located near the surface, whereas N* in the North Atlantic has a well-defined vertical maximum at depths of ~400 m. This difference is due in part to the advection of strong negative anomalies from the eastern denitrification zones. A shallow remineralization depth for N-rich organic matter due to more rapid remineralization of particles or a larger fraction going into the dissolved organic nitrogen pool may also contribute to the surface trapped N* signal.

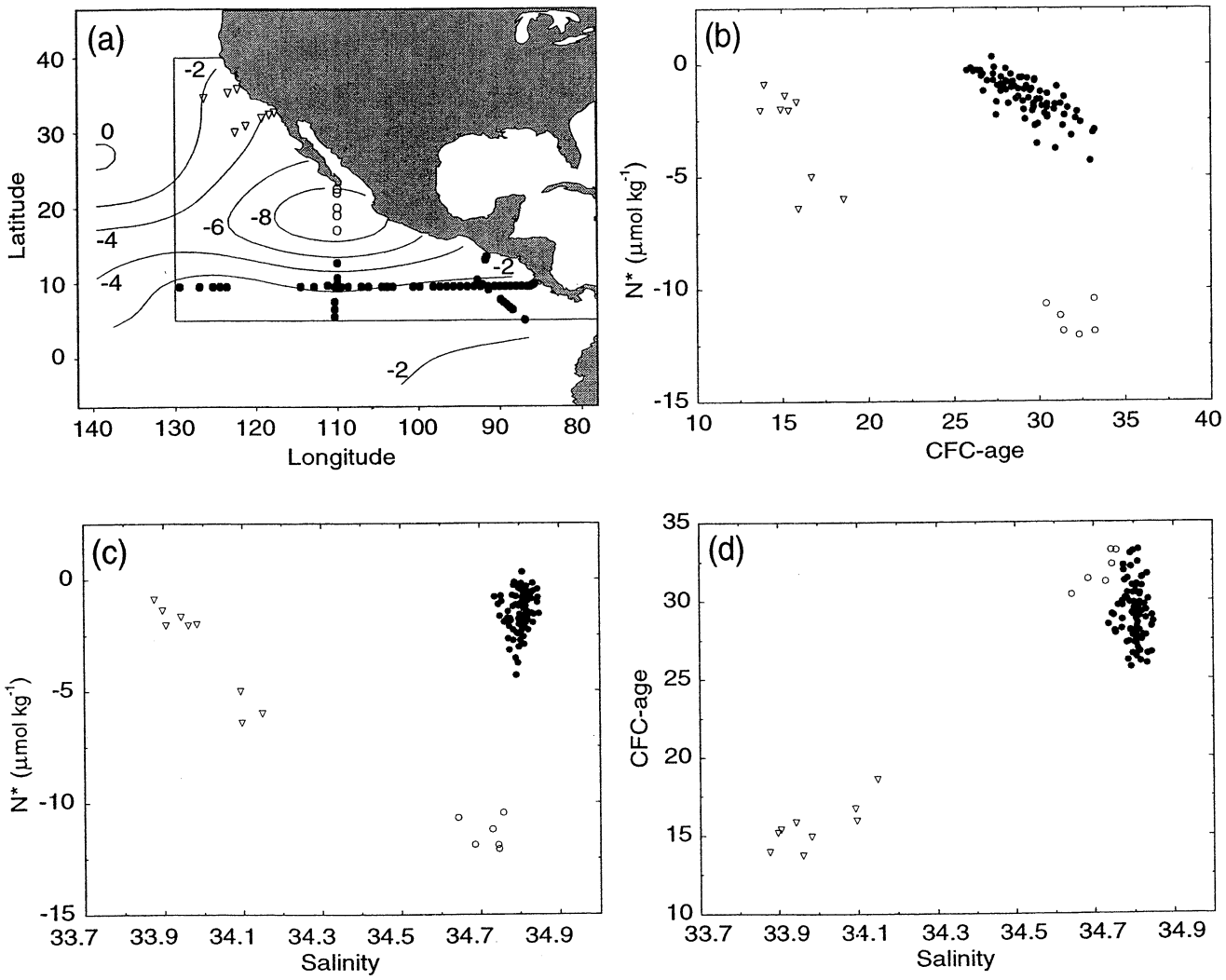

Figure 10. Same as Figure 9, except sigma-theta 26.4 in the ETNP.

Table 2. Estimated Values of the Rate of Change of N* on Isopycnal Surfaces

Layer	Rate[a]	σ_{rate}[b]	Observation	r^2	Volume,	Net N loss,
	$\mu mol/kg\ yr$		Number		10^{12} km^3	Tg N yr^{-1}
			ETSP			
25.80	-0.43	0.10	72	0.26	314	2.3
26.05	-1.02	0.11	70	0.62	222	3.7
26.20	-2.45	0.30	37	0.72	130	5.3
26.30	-2.01	0.41	43	0.44	153	5.1
26.40	-1.30	0.33	46	0.33	183	4.0
26.50	-0.84	0.20	52	0.27	222	3.1
26.60	-0.63	0.06	59	0.43	269	2.8
Total					1493	26.3
			ETNP			
25.80	-0.30	0.07	27	0.37	88	0.4
26.05	-0.39	0.06	44	0.51	108	0.7
26.20	-0.40	0.07	49	0.44	90	0.6
26.30	-0.46	0.06	69	0.54	134	1.0
26.40	-0.30	0.03	78	0.59	193	0.9
26.50	-0.47	0.04	60	0.75	276	2.1
26.60	-0.38	0.05	59	0.51	323	2.0
26.75	-0.52	0.17	25	0.35	324	2.8
Total					1536	10.7

[a]Slope of the linear regression of the form $\Delta N^* = a\ \Delta\tau + b$ (see equation (14)).

[b]1σ uncertainty of the slope a of this regression.

Furthermore, mixing processes at those depths are probably too complicated to be represented by such a simple end-member mixing model, which requires that source waters form with uniform N* values and mix predominantly along isopycnal surfaces. Source waters in the region of the N* maximum may form with heterogeneous N* values as a result of N* gradients across the water mass formation region or of strong interannual variability in thermocline ventilation. The nonlinear mixing of CFC-ages exacerbates this problem, since the younger ages found in the N* maximum are more strongly affected by curvature in the recent atmospheric history [*Doney et al.*, 1997] (see appendix C). We therefore estimate nitrogen fixation with the steady state form of (9) and an estimate of total N* divergence, to which we now proceeed.

4.3. Benthic Denitrification

For the contribution of benthic denitrification, we estimate an average areal denitrification rate for the Pacific continental shelf regions based on measurements reported by *Christensen et al.* [1987]. The average and standard error of rates compiled by *Christensen et al.* [1987] from the Mexican, Bering Sea, East China Sea, and Washington shelf regions is 0.38 ± 0.15 pmol N cm^{-2} s^{-1}, though some of the estimates were suggested to be too low, having failed to account for a nitrification/denitrification coupling. This is close to the global mean value of 0.44 pmol N cm^{-2} s^{-1} reported by *Wollast* [1991]. We calculate the shelf area of our region (depth less than 500 m, north of 32°S) based on the RAND Atlas [*Gates and Nelson*, 1975], resulting in a total shelf denitrification of 12 ± 5 Tg N yr^{-1}. We add to this half of the global deep benthic denitrification of ~6 Tg N yr^{-1} [*Liu and Kaplan*, 1984; *Hattori*, 1983] to get a total benthic denitrification of 15 ± 5 Tg N yr^{-1} in the Pacific north of 32°S. Owing to the likely underestimate of the areal rates, this should be regarded as a conservative estimate.

4.4. Ocean Transport

The nitrogen budget for an open basin requires knowledge of the total divergence of N* into the basin according to (9). The divergence of N*, not N, is the relevant

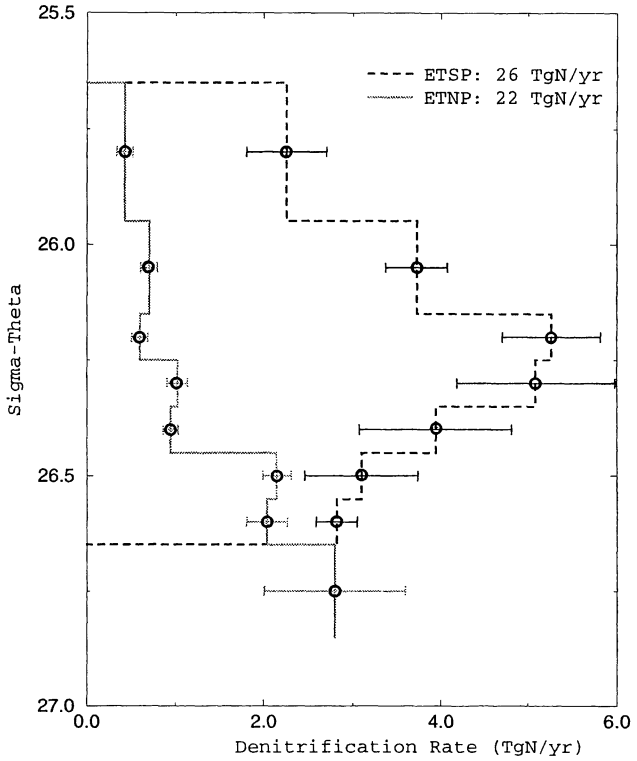

Figure 11. Integrated denitrification rate versus sigma-theta in the Eastern Tropical Pacific. The integrated denitrification rate of 22 Tg N yr^{-1} listed for the ETNP is double the rate for the depth interval shown (see text).

quantity for our purposes. This is because inorganic P divergences are related to convergences of organic nitrogen through the conservation of total phosphorus and the N:P ratio of organic matter. Thus N* divergence accounts for the contribution of inorganic and organic N divergences in the N budget (see appendix B). In this subsection we estimate the component of N* divergence due to water mass transport. This transport divergence consists of N* fluxes across a southern hydrographic section at 32°S and through the Bering and Indonesian Straits.

The transport divergence of N* is taken from an inverse box model of the global circulation by *Ganachaud and Wunsch* [2000], *Ganachaud and Wunsch* [2001]. The geostrophic interior circulation is derived from WOCE hydrographic data and the Jakarta Australia Dynamic Experiment, and the Ekman layer transport is obtained from annual mean wind stress of the NCEP/NCAR reanalysis [*Kalnay et al.*, 1996]. The solution is constrained to conserve mass, salt, top-to-bottom silica, heat and PO ($PO = 170\,P + O_2$) between hydrographic sections. Heat and PO are conserved only in layers that are not in contact with the surface.

The circulation solution has 16 Sv of net northward mass flow into the Pacific across 32°S. This is largely balanced by 15 Sv westward flow through the Indonesian passages. For the Bering Strait we assume a mass flow of 0.8 Sv out of the basin and compute the transport of N* with N and P concentrations from annual mean Levitus data in the Bering Strait.

The N* transports that result from this circulation are shown in Table 4. The N* transport through the south of the basin is nearly balanced by that through the Indonesian and Bering Straits. There is a small transport divergence of N* from the basin of $\sim 2 \pm 10$ Tg N yr^{-1}. The uncertainty of this divergence was calculated from the full error covariance of the global model of *Ganachaud and Wunsch* [2000], accounting for both oceanic variability and measurement errors. The N* transport divergence is small relative to the other budget terms, though its error is large.

The circulation solution described above implies a large divergence of P from the Pacific (Table 4). We therefore explored the sensitivity of these results to an imposed constraint of total phosphate conservation (top to bottom) in each box. From the literature, we esti-

Table 3. Comparison With Other Studies

Investigator	Nitrogen Loss, Tg N yr^{-1}	Method [a]
	Eastern Tropical North Pacific	
Codispoti [1973]	19	ETS activity
Codispoti [1973]	16	Mass transport
Codispoti and Richards [1976]	23	Mass transport
Codispoti and Richards [1976]	19	ETS activity
This study	22	N* with CFC-age
	Eastern Tropical South Pacific	
Tsunogai [1971]	3-7	
Elkins [1978]	18-26	
Codispoti and Packard [1980]	25	ETS activity
Codispoti and Packard [1980]	19	Mass transport
This study	26	N* with CFC-age

[a]Three methods have been used in these studies: in situ measurements of Electron Transport System (ETS) activity; transport of nitrate defecits (Mass Transport), and the N* CFC-age method in the current study (see section 4.1).

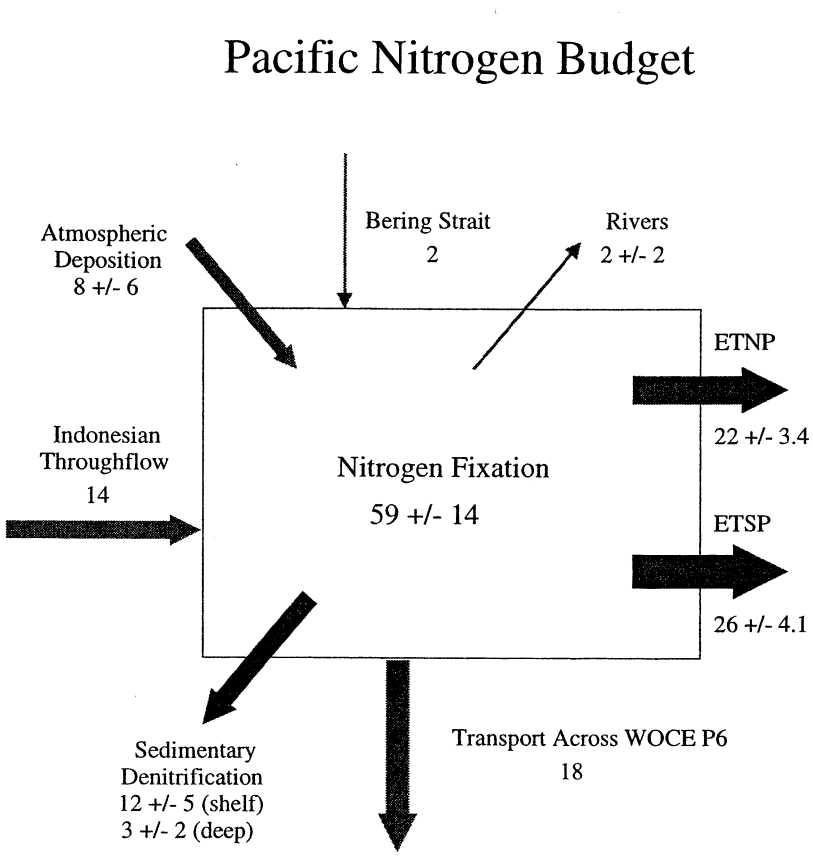

Figure 12. Estimated Pacific nitrogen budget. Light arrows represent N* transport terms; transports which act to increase (decrease) the N* of the basin are shown by inward (outward) pointing arrows. Dark arrows represent denitrification terms. Nitrogen fixation is the residual. Origins of the terms are given in Table 4.

mated atmospheric and riverine P inputs and calculated organic phosphate transport from profiles. Given the estimated P sources/sinks, the circulation was forced to conserve total P to within $\pm$ 0.5 Tg P yr^{-1} in each box. The N* divergence from that solution was nearly identical to the one already described. Since the P constraint is based on many highly uncertain estimates, we report in Table 4 the results from the solution without total P conservation.

4.5. Atmospheric Deposition and River Fluxes

To estimate the total N* divergence as required by (9) we must also include the contribution of atmospheric deposition at the sea surface and delivery from rivers. The atmospheric deposition of N consists of reduced and oxidized compounds. For oxidized N we use the model results of *Levy et al.* [1999], which yield an N deposition of 6 Tg N yr^{-1} in the area north of 32°S. These model results are comparable to the total Pacific oxidized N deposition calculated by *Duce et al.* [1991] based on atmospheric concentration measurements and deposition velocities.

For reduced nitrogen species we scale the Pacific ammonia deposition estimated by *Duce et al.* [1991] by the area of our region, giving 8.2 Tg N yr^{-1}. We subtract from this a recycled component due to the estimated 7 Tg N yr^{-1} of global oceanic ammonia emissions [*Dentener and Crutzen*, 1994], again scaled by area. This gives a net ammonia deposition of 6 Tg N yr^{-1} and a total atmospheric nitrogen deposition of 12 Tg N yr^{-1} for the region considered. The uncertainty of this number is difficult to constrain but we believe a 50% error to be an upper bound (H. Levy, personal communication, 1999). There is also a small atmospheric P deposition due to mineral aerosol, for which we use the *Duce et al.* [1991] value of 0.54 Tg P yr^{-1}.

For the contribution of rivers, we take the model results of *Seitzinger and Kroeze* [1998] for N delivery. These authors predict a Pacific riverine dissolved nitrogen discharge to estuaries of nearly 8 Tg N yr^{-1}. A significant portion of this is denitrified in continental margins before even reaching the coastal ocean. We adopt a value of 50% [*Seitzinger and Kroeze*, 1998], leaving a river transport of 4 Tg N yr^{-1} to the Pacific. We scale the global riverine P flux (2 Tg P yr^{-1} [*Howarth et al.*, 1995]) by the Pacific fraction of the global riverine N flux, giving a Pacific P flux of 0.86 Tg P yr^{-1}. Rivers thus contribute a small N* signal to the Pacific

Table 4. Pacific Marine Nitrogen Budget Estimate

Process	Magnitude, Tg yr^{-1}		
	N	P	N*
	Ocean Transport		
Transport across 32°S [a]	84	14.5	-18
Indonesian Throughflow [a]	-70	-12.0	14
Bering Strait [b]	- 4	-0.8	2
Transport Convergence	10	1.7	-2 ± 10
	Other Inputs		
Atmospheric deposition [c]	12 ± 6	0.5 ± 0.25	8 ± 6
River input [d]	4 ± 2	0.9 ± 0.45	-2 ± 2
Total Convergence	26	3.1	4 ± 12
	Denitrification		
Benthic denitrification [e]	15 ± 5		
Water column denitrification	48 ± 5		
	Nitrogen Fixation		
N_2 fixation [f]	59 ± 14		

[a]From an inverse box model of the global circulation [*Ganachaud and Wunsch*, 2000].
[b]Assuming a mass flux of 0.8 Sv and N and P concentrations averaged over the top 50 m from annual mean Levitus data.
[c]Based on *Levy et al.* [1999], *Duce et al.* [1991], and *Dentener and Crutzen* [1994]. We assume a 50% uncertainty in the N and P values individually.
[d]Based on model results of *Seitzinger and Kroeze* [1998], with half the river N flux denitrified in continental margins. We assume a 50% uncertainty in the N and P values.
[e]Based on rates from *Christensen et al.* [1987] and a Pacific shelf area from RAND Atlas.
[f]Calculated as residual of denitrification and N* convergence terms.

of about -2.0 ± 2 Tg N yr^{-1} (assuming independent 50% uncertainties in both N and P delivery).

The resulting N* sources from rivers and atmosphere are listed in Table 4, together with the transport divergence from the oceanic circulation. There is a combined convergence of N* through the boundaries of our region of 4 ± 12 Tg N yr^{-1}.

4.6. Budget Summary

We are now in a position to compile a budget of nitrogen for the Pacific north of 32°S using our N* divergence values from ocean transport, atmospheric deposition and river inputs, and our estimates of water column and sedimentary denitrification. Inserting these into (9), we find that there is an imbalance of -59 ± 14 Tg N yr^{-1} between the nitrogen loss from denitrification and the supply from the atmosphere, rivers, and large-scale circulation. A balanced budget would thus require nitrogen fixation to supply 59 ± 14 Tg N yr^{-1} over the region from 32°S to the Bering Strait. The large-scale high N* anomalies in the tropics and subtropics, together with direct independent estimates of nitrogen fixation rates and *Trichodesmium sp.* abundance clearly indicate that nitrogen fixation is compensating some of those losses.

However, imbalances between nitrogen fixation, denitrification, and convergence of N* cannot be ruled out. Such imbalances would result in a temporal trend in the integrated N* (or the average N:P ratio) of the basin. This potential non steady state behavior of the Pacific mean N* presents a source of error that is difficult to constrain.

The timescale we are interested in with respect to such imbalances is the timescale for which the other elements of our budget are estimated, namely the past couple decades. We are aware of two types of investigation into changes in the Pacific N:P ratio for that time period. First, data from the time series station at Aloha has revealed an increase since 1988 in the shallow (above 100 m) N:P ratio of suspended particles [*Karl et al.*, 1997]. However, there has been no concurrent increase in total dissolved N:P ratios in the top 500 m, which comprises over 95% of the shallow nitrogen pool. Second, a recent comparison of N and P measurements between historical data and WOCE data in the mid-depth North Pacific (~1000-2000 m) [*Pahlow and Riebesell*, 2000] found no significant large-scale changes in the N:P ratio. This study complements the findings of constant dissolved N:P ratios at Aloha and supports the conclusion that the mean Pacific N:P ratio has not changed significantly in recent decades.

Although our estimate of nitrogen fixation is derived

for the basin scale, the N* distribution itself gives insight into the spatial distribution of the nitrogen fixation sources. We reiterate that care must be taken in inferring locations of nitrogen fixation (or denitrification) from N* patterns alone, since N* records the net accumulation or diminution of excess N in a water mass. In the present discussion, for example, it would be incorrect to conclude solely on the basis of N* that nitrogen fixation is occuring only in the region of high N* in the tropical to subtropical western basin. It may be that fixation exists in the ETSP and ETNP, for example, but is simply overwhelmed by the strong denitrification signal. However, on the basis of other factors, including the observed distribution of *Trichodesmium sp.* in the Pacific [*Carpenter*, 1983] and the large source of surface nitrate in the east from upwelling, we conclude that this is not the case. That is, nitrogen fixation in the Pacific is not uniformly distributed, but instead occurs primarily in the western (to ~140°W) part of the subtropical gyres as suggested by the N* distribution.

It is interesting to consider the factors that are responsible for the observed locations of nitrogen fixation. The high N* anomalies of the Pacific lie in the tropical and subtropical latitudes. This feature can be explained by the ability of *Trichodesmium sp.* colonies to thrive only in warm (> 20°C), saline waters [*Capone et al.*, 1997]. Oligotrophy also helps to create a competitive environment for nitrogen fixation. The low-latitude location of the high N* region is therefore not surprising. However, these considerations are not able to explain why high near-surface N* anomalies should be found only in the western part of the basin.

It has been hypothesized that iron may limit the growth of diazotrophic organisms [*Rueter et al.*, 1992] and therefore the location and magnitude of oceanic nitrogen fixation [*Falkowski*, 1997]. The iron supply to the surface ocean has been proposed to derive largely from deposition of dust from the atmosphere [*Duce et al.*, 1991]. Although in some regions, the primary iron source is upwelling and entrainment, the recent study by *Fung et al.* [2000] shows that atmospheric inputs dominate in the Pacific north of 40°S. The large-scale patterns of dust deposition and N* thus provide the means to examine hypotheses about the importance of iron as a control on nitrogen fixation.

Maps of dust delivery to the surface waters of the Pacific [*Tegen and Fung*, 1994] show some similarity in spatial pattern to the locations of nitrogen fixation inferred from the N* distribution. That is, atmospheric iron supply is highest in the western part of the basin where dust lifted from soils of Asia and Australia settles or is washed out of the prevailing westerly winds at the latitudes of the subtropical gyres. *Gruber and Sarmiento* [1997] found a similar situation in the Atlantic. The dominant horizontal N* gradients in the Atlantic were meridional and again resembled those of dust deposition. These findings do not constitute proof that oceanic nitrogen fixation is limited by iron supply but, taken together with fundamental physiological constraints, support iron limitation of nitrogen fixation as a sound working hypothesis.

Our inferences about the distribution of nitrogen fixation are also consistent with the isotopic composition of nitrogen. On the basis of nitrogen isotopes, *Saino and Hattori* [1987] concluded that nitrogen fixation occurs mainly in the western part of the basin. These authors examined the geographical variations in the isotopic composition of particulate organic nitrogen. They found that N in the subsurface of the western Pacific was depleted in ^{15}N relative to the eastern Pacific and attributed this to the input of isotopically light dissolved N_2 gas, which experiences no significant fractionation during fixation. The isotopic composition of N was also examined by *Liu et al.* [1996] for Kuroshio waters in which the subsurface pool of isotopically light N is interpreted as deriving from diazotrophic organic matter.

We know of no previous basin-scale geochemical estimates of nitrogen fixation in the Pacific. There are, however, estimates on a regional scale with which we can compare our results. *Karl et al.* [1997] present various estimates of nitrogen fixation from time series data collected at ocean station Aloha, near Hawaii. These include observations of *Trichodesmium sp.* abundance, acetylene reduction as a proxy for nitrogen fixation, and isotopic and N:P mass balances. The range of values is between 31-51 mmol N m^{-2} yr^{-1}. Smaller rates of 13 mmol N m^{-2} yr^{-1} have been calculated by *Liu et al.* [1996] based on isotopic mass balances in Kuroshio waters. Assuming that our estimate of 59 ± 14 Tg N yr^{-1} is confined to the region from 30°N to 30°S (corresponding roughly to surface waters with annual average temperatures above 20°), yields an average areal rate of 39 ± 9 mmol N m^{-2} yr^{-1}. This is quite close to the average value of all estimates presented by *Karl et al.* [1997], and about half the areal rates found for the North Atlantic by *Gruber and Sarmiento* [1997].

Finally, we note that the Pacific N budget presented here agrees quite well with the extrapolation of *Gruber and Sarmiento* [1997], which attributed ~55 Tg N yr^{-1} of nitrogen fixation to the Pacific. Our uncertainties still do not permit a definitive answer about the degree of balance between sources and sinks of nitrogen in the modern ocean. However, the current study supports the view presented by *Gruber and Sarmiento* [1997] of a N cycle which has large sources of newly fixed N which are in approximate balance with losses.

5. Summary and Outlook

We have presented a nitrogen budget for the Pacific based on the quasi-conservative tracer, N* calculated

Table 5. Summary of Cruises

Cruise[a]	Dates	Ship, Country
GEOSECS	Aug 1973 to May 1974	Melville, United States
TPS47 (P1)	Aug 1985 to Sep 1985	T. Thompson, United States
TPS24 (P3)	Mar 1983 to Jun 1985	T. Thompson, United States
TPS10 (P4)	Feb 1989 to May 1989	Maona Wave, United States
P6	May 1992 to Jul 1992	Knorr, United States
P9	Jul 1994 to Aug 1994	Ryofu Maru, Japan
P10	Oct 1993 to Nov 1993	T. Thompson, United States
P11S	Jun 1993 to Jul 1993	Franklin, Australia
P13	Aug 1992 to Oct 1992	J.V. Vickers, United States
P14N	Jul 1993 to Sep 1993	T. Thompson, United States
P14C	Sep 1992	Knorr, United States
P14S,P15S	Jan 1996 to Feb 1996	Discoverer, United States
P15N	Sep 1994 to Nov 1994	J.P. Tully, Canada
P16N	Feb 1991 to Apr 1991	Discoverer, United States
P16C	Aug 1991 to Oct 1991	T. Washington, United States
P16S,P17S	Jul 1991 to Aug 1991	T. Washington, United States
P16A,P17A	Oct 1992 to Nov 1992	Knorr, United States
P17N	May 1993 to Jun 1993	T. Thompson, United States
P17C	May 1991 to Jul 1991	T. Washington, United States
P17E,P19S	Dec 1992 to Jan 1993	Knorr, United States
P19C	Feb 1993 to Apr 1993	Knorr, United States
P18	Feb 1994 to Apr 1994	Discoverer, United States
P19C	Feb 1993 to Apr 1993	Knorr, United States
P21	Mar 1994 to Jun 1994	Melville, United States
P31	Jan 1994 to Feb 1994	T. Thompson, United States
S4P	Feb 1992 to Apr 1992	Akademik Ioffe, Russia

[a]All cruises are from WOCE (World Ocean Circulation Experiment) except GEOSECS (Geochemical Ocean Sections Study).

from the newly available WOCE nutrient data. Using N* in conjunction with age tracers, we are able to estimate spatially and temporally integrated rates of denitrification in the Eastern Tropical Pacific of 48 Tg N yr^{-1}.

The distribution of N* reveals the tropical and subtropical Pacific as important regions in the global supply of oceanic fixed nitrogen. By estimating the divergence of N* to the basin, we calculate that biological nitrogen fixation would be required to fix 59 Tg N annually, to balance the large losses due to denitrification.

The apparent dominance of the western basin for supplying this newly fixed nitrogen supports the working hypothesis that iron is a limiting factor for nitrogen fixation. However, this inference is at present based on rather qualitative similarities in the distribution of iron deposition and N* concentration.

Much work still needs to be done to more precisely determine the nature of the relationships between nitrogen fixation and iron supply. Until then, questions about the role of glacial to interglacial changes in oceanic N inventory as a result of changes in dust flux will remain speculative.

Appendix A: Internal Data Consistency

We investigate the internal consistency of the Pacific WOCE data by determining deep ocean (>3500 m) N and P trends versus potential temperature at stations that were reoccupied or closely revisited by different cruises. The WOCE cruises used in this study were completed from March 30, 1985, through June 30, 1996, and are listed in Table 5. We assume here that water mass properties below 3500 m show little temporal variability over the 11 year range of data collection and that mean offsets between any cruise and its intersecting cruises are therefore due to analytical inconsistencies. The 49 cruise intersections we examined are indicated on Figure 1.

The stations used at each intersection were chosen to provide enough samples for comparison without introducing "real" measurement differences due to distances between stations. The largest separation between stations was 4°, but most were less than 2°apart.

Deep water P and N at intersections were then plotted against potential temperature to provide a check against the presumption that the same water mass was sampled by each cruise. Offsets for the intersection were assigned for each nutrient based on the difference between the best fit lines for intersecting cruises (Figure A1). Finally, for each cruise we used offsets for all its intersections (Figures A2-A3) to calculate a mean offset for both P and N.

For those cruises with mean offsets that exceeded 4 times the analytical precision, "corrections" were introduced. We applied three such corrections to the nutri-

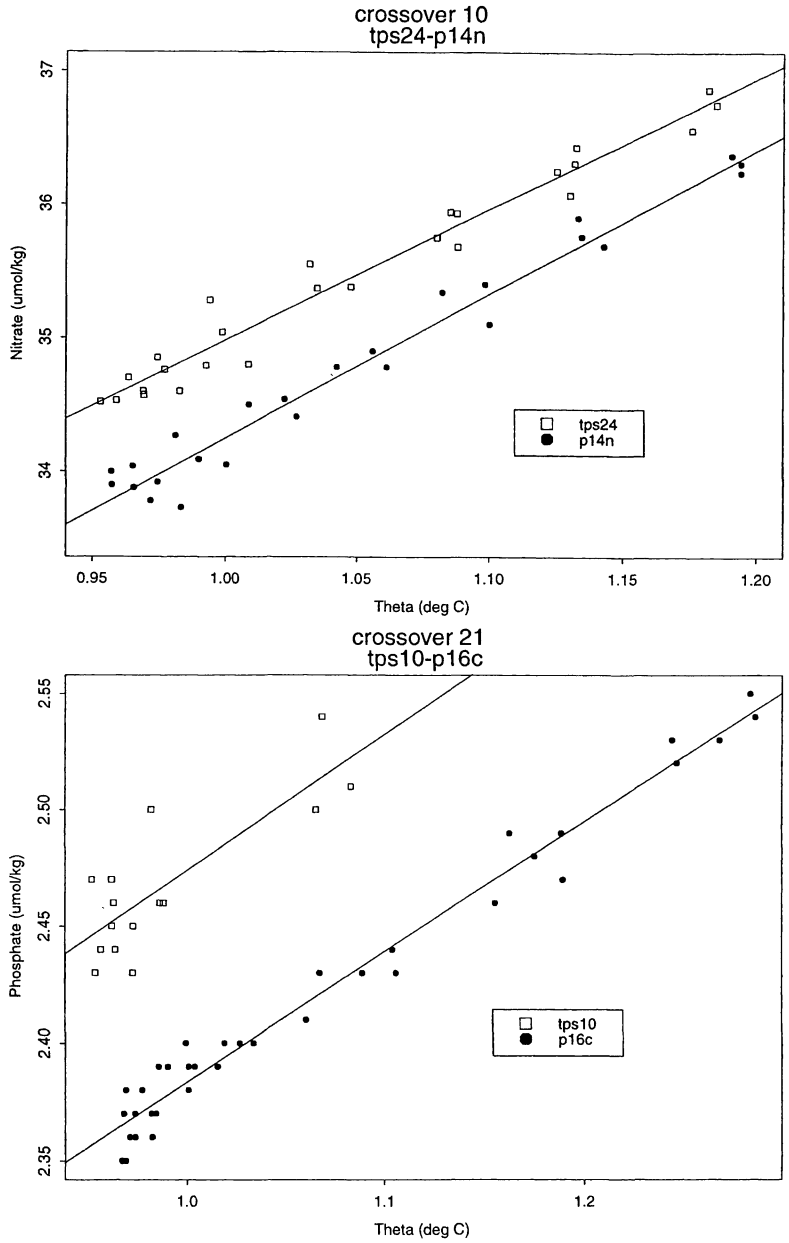

Figure A1. (top) Nitrate versus potential temperature (theta) at the intersection between cruises TPS24 and P14N for depths below 3500 m. Data from P14N are shown by solid circles, and data from TPS24 are shown by open squares. The solid lines (both figures) represent the results of a linear regression. A mean nitrate difference of 0.6 μmol kg^{-1} was found between TPS24 and intersecting cruises. (bottom) Phosphate versus potential temperature at the intersection between cruises TPS10 and P16C for depths below 3500 m. Data from P16C are shown by solid circles, and data from TPS10 are shown by open squares. A mean phosphate difference of 0.04 μmol kg^{-1} was found between TPS10 and intersecting cruises.

ent data:

$$\begin{aligned} \text{cruise TPS10} &: N_{\text{corr}} = N_{\text{meas}} - 0.7\ \mu\text{mol kg}^{-1}, \\ \text{cruise TPS24} &: N_{\text{corr}} = N_{\text{meas}} - 0.6\ \mu\text{mol kg}^{-1}, \\ \text{cruise TPS24} &: P_{\text{corr}} = P_{\text{meas}} + 0.04\ \mu\text{mol kg}^{-1}. \end{aligned}$$

Appendix B: N* Continuity Equation

We elaborate here on the geochemical meaning of (9). We wish to explain the relevance of P divergence for our N budget, by illustrating its connection to the divergence of total fixed nitrogen (which one may regard as the more obviously relevant quantity for a study of the fixed nitrogen budget). That is, we will show that the P divergence in (9) acts as a substitute for organic nitrogen divergence. We begin by noting that in principle, one could estimate a nitrogen budget based directly on the conservation of total fixed nitrogen, TN (TN = N + TON, where TON is total organic nitrogen), in which

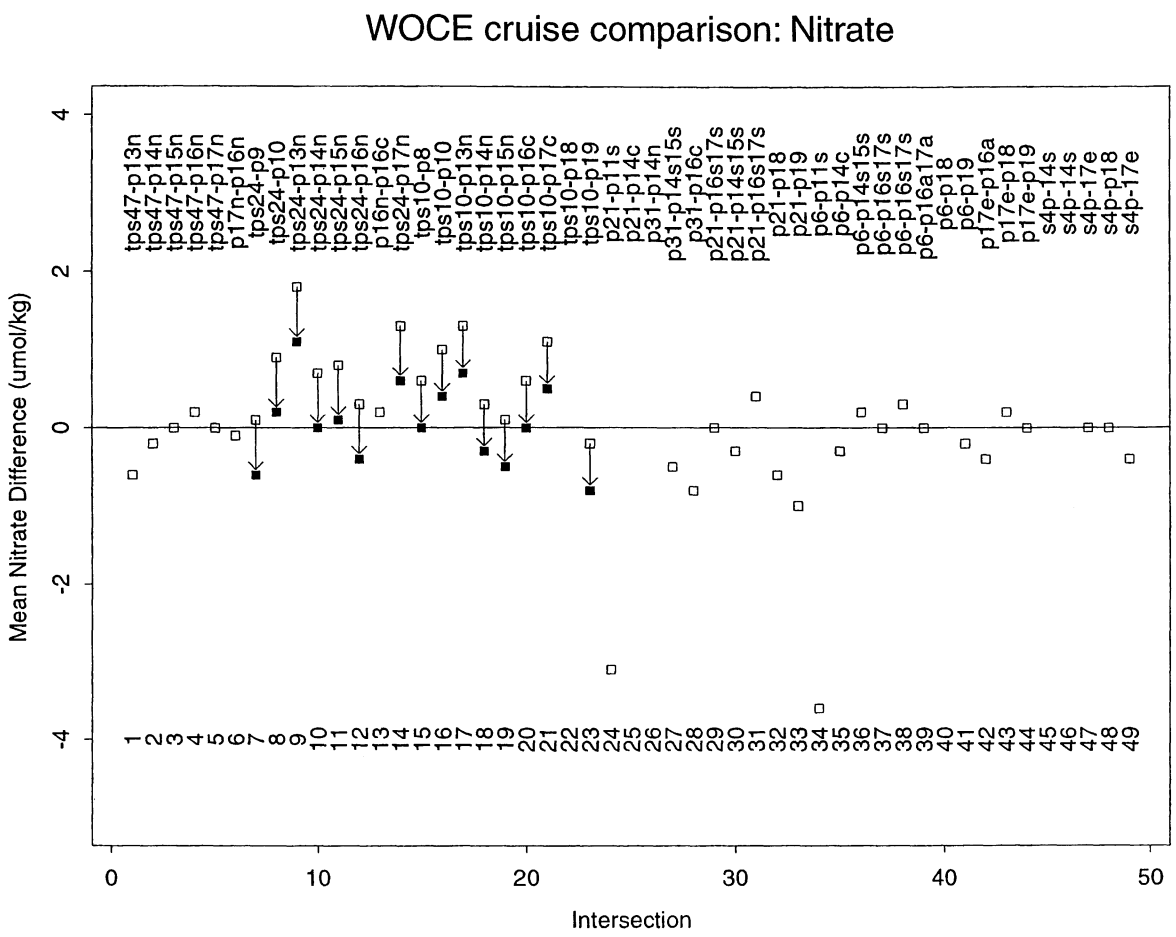

Figure A2. Nitrate offset versus cruise intersection. Intersection numbers and locations are shown in Figure 1. Open and filled squares are the intersection offsets before and after corrections were applied, respectively.

nitrification terms play no role since they only involve exchanges between N and TON. The conservation of TON may be written

$$\Gamma(\mathrm{TON}) = J_{\mathrm{nitr}}(\mathrm{TON}) + J_{\mathrm{denit}}(\mathrm{TON}) + J_{\text{N-rich}}(\mathrm{TON}) + J_{\text{up nf}}(\mathrm{TON}). \quad \text{(B1)}$$

This is identical to the corresponding inorganic equation (1), except that TON has an additional source due to uptake of N_2 by diazotrophs. Terms 1 and 3 on the right-hand side of (B1) are equal in magnitude and opposite in sign to the corresponding terms in (1), whereas the denitrification terms are both sinks.

If we now add the organic equation and the inorganic equation in steady state integral form, we get

$$\int_S \Gamma(\mathrm{TN})\, dS = \int_S [\Gamma(\mathrm{N}) + \Gamma(\mathrm{TON})]\, dS = \int_V [J_{\mathrm{denit}}(\mathrm{TON}) + J_{\mathrm{denit}}(\mathrm{N}) + J_{\text{up nf}}(\mathrm{TON})]\, dV. \quad \text{(B2)}$$

Establishing a nitrogen budget based on (B2) would indeed be a more intuitive approach than (9). However, we lack sufficient information about TON across the Pacific to calculate its transport into the basin. We would like to show now that the content of the two approaches ((9) and (B2)) is identical. In other words we may use P rather than TON to eliminate the effects of nitrification, which gives an N* based budget for total nitrogen that is equivalent to (B2) but requires no direct information about TON.

Recall from section 2 that the coefficient of the denitrification source term in (9) accounts for denitrification of both N and TON, so that the right-hand sides of (9) and (B2) are identical. For the left-hand sides, we note the following. For regions in which the uptake and remineralization of P from diazotrophs are balanced, there can be no net convergence or divergence of diazotrophic organic matter, so convergences of TON and TOP must occur with the ratio $r_{\mathrm{nitr}}^{\mathrm{N:P}}$. Since total phosphorus must be conserved, we also know that a convergence of P must be balanced by a divergence of total organic phosphorus. Combining these two statements, we can write

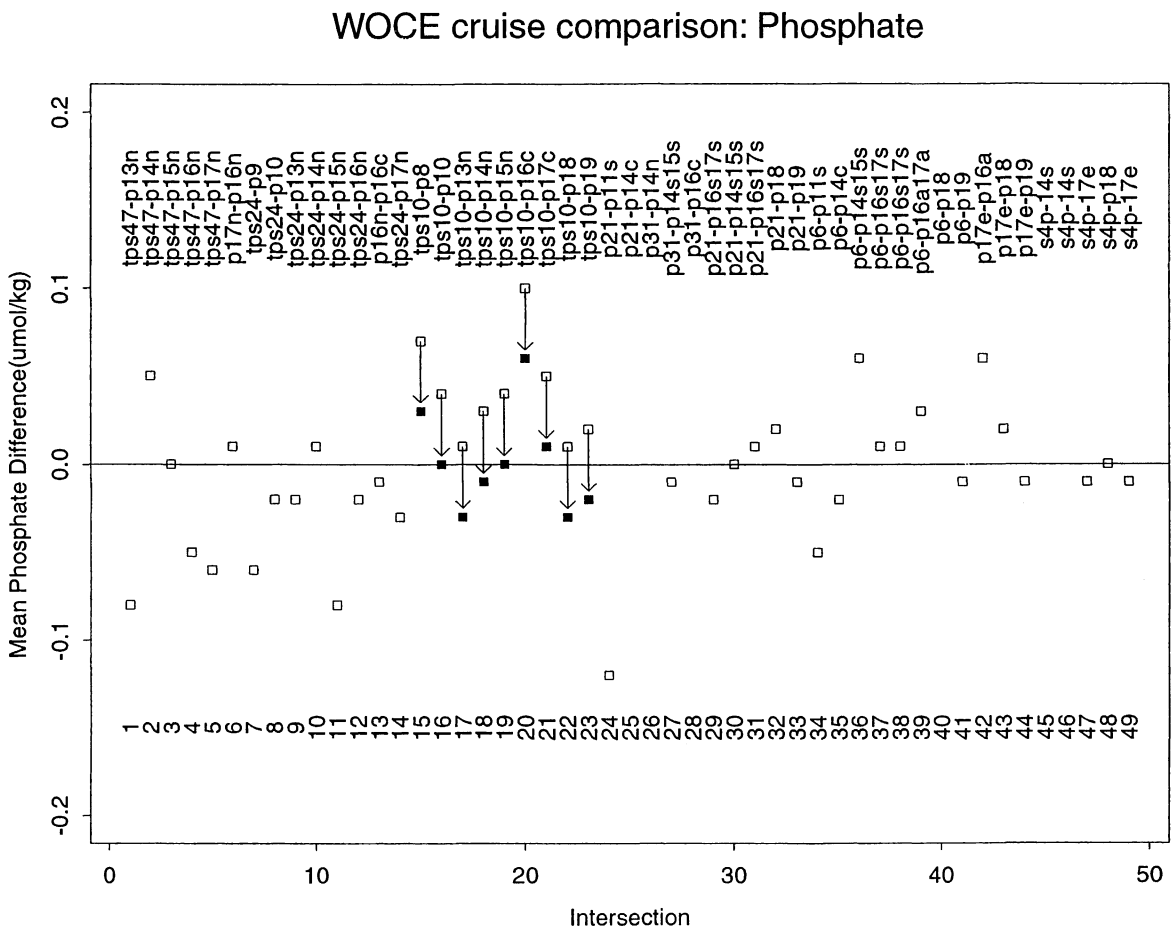

Figure A3. Phosphate offset versus cruise intersection. Symbols are as in figure A2.

$\int_S \Gamma(\mathrm{TON})\, dS = -r^{\mathrm{N:P}}_{\mathrm{nitr}} \int_S \Gamma(\mathrm{P})\, dS$. Thus we see that the P divergence in the N* continuity (9) takes the place of TON convergence in (B2). Our budget based on N* is therefore identical to that for TN but has the advantage of being calculable from inorganic nutrient data only.

Appendix C: Water Mass Ages

The age of a water mass, defined as the time elapsed since it was at the surface, is estimated by matching CFC-12 concentrations to the atmospheric history of CFC-12 partial pressure (see *Fine* [1995] for a review). Since the error of the CFC-age estimate increases with increasing age [*Doney et al.*, 1997], we use only waters with CFC-ages 40 years or less.

Undersaturation of the water parcel with respect to the atmosphere at the time of water parcel isolation will lead to an overestimate of the age. Since we will only be interested in aging of parcels, and not in the absolute age, this effect will have very little influence on our results. In other words, the value of CFC-age assigned at the outcrop is irrelevant for our purposes, since we are interested only in CFC-age gradients.

Mixing of CFC-ages introduces a further deviation from age behavior. For CFC-ages, the nonconservative component ($\Delta\tau$) of a mixture's age (13) has two contributions in addition to the aging of the mixture [*Warner et al.*, 1996]. That is, two factors prevent CFC-age from mixing linearly, as would an age tracer. First the solubility of CFC-12 is not a linear function of temperature and salinity. However, over the ranges of T and S with which we will be concerned, this introduces a negligible (~1%) error in CFC partial pressure. More importantly, the atmospheric rate of increase has not been constant, which means that a mixture of two water masses has an age that is different from the mixed age to a degree that depends on the curvature of the atmospheric increase [*Doney et al.*, 1997]. We estimate that this effect introduces a systematic error of up to 10% for the range of ages considered here; highest error occurs for the mixing of end members with the greatest age difference. Since these errors in the interpretation of our calculated ($\Delta\tau$) are rather difficult to quantify in

general, we add the upper limit of 10% uncertainty to the result of our denitrification rate estimates.

Acknowledgments. We wish to express our sincere appreciation for all the scientists and personnel involved in the collection and analysis of the high quality data from the WOCE program, without which this study would not have been possible. Financial support for C.D. and J.L.S. was provided by grants from NOAA (NA56GP0439) and NSF (OCE-9617972). N.G. was supported by a NOAA Global and Climate Change fellowship. A.G. was supported by Jet Propulsion Laboratory (contract 958125) and the American Auto Manufacturers Association, through the MIT Center for Global Change Sciences.

References

Altabet, M. A., R. Francois, D. W. Murray, and W. L. Prell, Climate-related variations in denitrification in the Arabian Sea from sediment $^{15}N/^{14}N$ ratios, *Nature, 373*, 506–509, 1995.

Anderson, L. A., On the hydrogen and oxygen content of marine phytoplankton, *Deep Sea Res., Part I, 42*(9), 1675–1680, 1995.

Anderson, L. A., and J. L. Sarmiento, Redfield ratios of remineralization determined by nutrient data analysis, *Global Biogeochem. Cycles, 8*(1), 65–80, 1994.

Barnes, R. O., K. K. Bertine, and E. D. Goldberg, N_2:Ar, nitrification and denitrification in southern California borderland basin sediments, *Limnol. Oceanogr., 20*(6), 963–970, 1975.

Brandhorst, W., Nitrification and denitrification in the eastern tropical North Pacific, *J. Cons. Explor. Mer, 25*, 3–20, 1959.

Broecker, W. S., and G. M. Henderson, The sequence of events surrounding Termination II and their implications for the cause of glacial-interglacial CO_2 changes, *Paleoceanography, 13*(4), 352–364, 1998.

Capone, D. G., J. P. Zehr, H. W. Paerl, B. Bergman, and E. J. Carpenter, Trichodesmium, a globally significant marine cyanobacterium, *Science, 276*, 1221–1229, 1997.

Carpenter, E. J., Nitrogen fixation by marine Oscillatoria (*Trichodesmium*) in the world's oceans, in *Nitrogen in the marine environment*, edited by E. J. Carpenter and D. G. Capone, pp. 65–103, Academic, San Diego, Calif., 1983.

Christensen, J. P., J. W. Murray, A. H. Devol, and L. A. Codispoti, Denitrification in continental shelf sediments has major impact on the oceanic nitrogen budget, *Global Biogeochem. Cycles, 1*(2), 97–116, 1987.

Codispoti, L. A., *Denitrification in the Eastern Tropical North Pacific.*, Ph. D. thesis, Univ. of Washington, Seattle, 1973.

Codispoti, L. A., Phosphorus vs. nitrogen limitation of new and export production, in *Productivity of the Ocean: Present and Past*, edited by W. H. Berger, V. S. Smetacek, and G. Wefer, pp. 377–394, John Wiley, New York, 1989.

Codispoti, L. A., and T. T. Packard, Denitrification rates in the eastern tropical south Pacific, *J. Mar. Res., 38*(3), 453–477, 1980.

Codispoti, L. A., and F. A. Richards, An analysis of the horizontal regime of denitrification in the eastern tropical North Pacific, *Limnol. Oceanogr., 21*(3), 379–388, 1976.

Dentener, F., and P. Crutzen, A 3-dimensional model of the global ammonia cycle, *J. Atmos. Chem., 19*(4), 331–369, 1994.

Doney, S. C., W. J. Jenkins, and J. L. Bullister, A comparison of ocean tracer dating techniques on a meridional section in the eastern North Atlantic, *Deep Sea Res., Part I, 44*(4), 603–626, 1997.

Duce, R. A., et al., The atmospheric input of trace species to the world ocean, *Global Biogeochem. Cycles, 5*(3), 193–259, 1991.

Elkins, J., *Aquatic Sources and Sinks for Nitrous Oxide.*, Ph. D. thesis, Harvard University, Cambridge, Mass, 1978.

Falkowski, P. G., Evolution of the nitrogen cycle and its influence on the biological sequestration of CO_2 in the ocean, *Nature, 387*, 272–275, 1997.

Fine, R. A., Tracers, time scales, and the thermohaline circulation: The lower limb in the North Atlantic ocean, *U.S. Natl. Rep. Int. Union Geod. Geophys. 1991-1994, Rev. Geophys., 33*, 1353–1365, 1995.

Fung, I. Y., S. K. Meyn, I. Tegen, S. C. Doney, J. G. John, and J. K. B. Bishop, Iron supply and demand in the upper ocean, *Global Biogeochem. Cycles, 14*(1), 281–295, 2000.

Ganachaud, A., and C. Wunsch, Improved estimates of global ocean circulation, heat transport and mixing from hydrographic data, *Nature, 408*, 453–457, 2000.

Ganachaud, A., and C. Wunsch, Oceanic nutrient and oxygen fluxes during the world ocean circulation experiment and boundaries on export production, *Global Biogeochem. Cycles*, in press, 2001.

Ganachaud, A., and C. Wunsch, Oceanic nutrient and oxygen fluxes during the world ocean circulation experiment and boundaries on export production, *Global Biogeochem. Cycles*, in press, 2001.

Ganeshram, R. S., T. F. Pedersen, S. E. Calvert, and J. W. Murray, Large changes in oceanic nutrient inventories from glacial to interglacial periods, *Nature, 376*, 755–758, 1995.

Gates, W., and A. Nelson, A new (revised) tabulation of the Scripps topography on a 1 degree global grid, Tech. Rep. II: Ocean Depths, The Rand Corp., Santa Monica, Calif., 1975.

Gruber, N., and J. L. Sarmiento, Global patterns of marine nitrogen fixation and denitrification, *Global Biogeochem. Cycles, 11*(2), 235–266, 1997.

Haines, J., R. Atlas, R. Griffiths, and R. Morita, Denitrification and nitrogen fixation in Alaskan continental shelf sediments, *Appl. Environ. Microbiol., 41*, 412–421, 1981.

Hattori, A., Denitrification and dissimilatory nitrate reduction, in *Nitrogen in the Marine Environment*, edited by E. J. Carpenter and D. G. Capone, pp. 191–232, Academic, San Diego, Calif., 1983.

Howarth, R. W., H. Jensen, R. Marino, and H. Postma, Transport and processing of phosphorus in near-shore and oceanic waters, in *Phosphorus in the Global Environment*, edited by H. Tiessen, pp. 323–345, John Wiley, New York, 1995.

Jahnke, R. A., C. E. Reimers, and D. B. Craven, Intensification of recycling of organic matter at the sea floor near ocean margins, *Nature, 348*, 50–54, 1990.

Kalnay, E., et al., The NCEP/NCAR 40-year reanalysis project, *Bull. Am. Meteorol. Soc., 77*(3), 437–471, 1996.

Karl, D. M., R. Letelier, D. V. Hebel, D. F. Bird, and C. D. Winn, Trichodesmium blooms and new production in the North Pacific gyre, in *Marine Pelagic Cyanobacteria: Trichodesmium and Other Diazotrophs*, edited by E. J. Carpenter, pp. 219–237, Kluwer Acad., Norwell, Mass., 1992.

Karl, D. M., R. Letelier, L. Tupas, J. Dore, J. Christian, and D. Hebel, The role of nitrogen fixation in the biogeo-

chemical cycling in the subtropical north pacific ocean, *Nature, 388*, 533–538, 1997.

Key, R. M., P. D. Quay, G. A. Jones, A. P. McNichol, K. F. VonReden, and R. J. Schneider, WOCE AMS radiocarbon I: Pacific Ocean results (P6, P16 and P17), *Radiocarbon, 38*(3), 425–518, 1996.

Koike, I., and A. Hattori, Estimates of denitrification in sediments of the Bering Sea shelf, *Deep Sea Res., Part A, 26*, 409–415, 1979.

LeTraon, P. Y., A method for optimal analysis of fields with spatially variable mean, *J. Geophys. Res., 95*, 13,543–13,547, 1990.

Levitus, S., and T. P. Boyer, World Ocean Atlas 1994, Tech. Rep. vol. 4, Temperature, Natl. Oceanic and Atmos. Admin., Silver Spring, Md., 1994.

Levitus, S., R. Burgett, and T. Boyer, World Ocean Atlas 1994, Tech. Rep. vol. 3, Salinity, Natl. Oceanic and Atmos. Admin., Silver Spring, Md., 1994.

Levy, H., W. Moxim, A. Klonecki, and P. Kasibhatla, Simulated tropospheric NO_x: Its evaluation, global distribution, and individual source contributions, *J. Geophys. Res., 104*, 26,279–26,306, 1999.

Liu, K.-K., and I. Kaplan, Denitrification rates and availability of organic matter in marine environments, *Earth Planet. Sci. Lett., 68*, 88–100, 1984.

Liu, K.-K., M.-J. Su, C.-R. Hsueh, and G.-C. Gong, The nitrogen isotopic composition of nitrate in the Kuroshio Water northeast of Taiwan: Evidence for nitrogen fixation as a source of isotopically light nitrate, *Mar. Chem., 54*, 273–292, 1996.

McElroy, M. B., Marine biological controls on atmospheric CO_2 and climate, *Nature, 302*, 328–329, 1983.

Pahlow, M., and U. Riebesell, Temporal trends in deep ocean Redfield ratios, *Science, 287*, 831–833, 2000.

Rueter, J. G., D. A. Hutchins, R. W. Smith, and N. L. Unsworth, Iron nutrition of Trichodesmium, in *Marine Pelagic Cyanobacteria: Trichodesmium and Other Diazotrophs*, edited by E. J. Carpenter, pp. 289–306, Kluwer Acad., Norwell Mass., 1992.

Saino, T., and A. Hattori, Geographical variation of the water column distribution of suspended particulate organic nitrogen and its n15 natural abundance in the Pacific and its marginal seas, *Deep Sea Res., 34*, 807–827, 1987.

Seitzinger, S., and C. Kroeze, Global distribution of nitrous oxide production and N inputs in freshwater and coastal marine ecosystems, *Global Biogeochem. Cycles, 12*(1), 93–113, 1998.

Tegen, I., and I. Fung, Modeling of mineral dust in the atmosphere: Sources, transport and optical thickness, *J. Geophys. Res., 99*, 22,897–22,914, 1994.

Tsunogai, S., Ammonia in the oceanic atmosphere and the cycle of nitrogen compounds through the atmosphere and hydrosphere., *Geochem. J., 5*, 57–67, 1971.

Tsunogai, S., M. Kusakabe, H. Iizumi, I. Koike, and A. Hattori, Hydrographic features of the deep water of the Bering Sea - the sea of silica, *Deep Sea Res., Part A, 26*(6), 641–659, 1979.

Tyrell, T., The relative influences of nitrogen and phosphorus on oceanic primary production, *Nature, 400*, 525–531, 1999.

Warner, M. J., J. L. Bullister, D. P. Wisegarver, R. H. Gammon, and R. F. Weiss, Basin-wide distributions of chlorofluorocarbons CFC-11 and CFC-12 in the North Pacific: 1985-1989, *J. Geophys. Res., 101*, 20,525–20,542, 1996.

Wollast, R., The coastal organic carbon cycle: Fluxes, sources and sinks., in *Ocean Margin Processes in Global Change*, edited by R. Mantoura, J.-M. Martin, and R. Wollast, pp. 365–381, John Wiley, New York, 1991.

Wyrtki, K., Circulation and water masses in the eastern equatorial Pacific Ocean, *Int. J. Oceanol. Limnol., 1*(1), 117–147, 1967.

C. Deutsch, N. Gruber, R.M. Key, and J.L. Sarmiento, Program in Atmospheric and Oceanic Sciences, Princeton University, Princeton, NJ 08544-0710. (cdeutsch@splash.princeton.edu; ngruber@igpp.ucla.edu; key@splash.princeton.edu; jls@splash.princeton.edu)

A. Ganachaud, Massachusetts Institute of Technology/Woods Hole Oceanographic Institute Joint Program, Cambridge, Massachusetts, 02139. (Alexandre.Ganachaud@ifremer.fr)

(Received April 18, 2000; revised November 13, 2000; accepted December 18, 2000.)